DIGITALCOMMONS
—@WAYNESTATE—

Wayne State University

Wayne State University Theses

1-1-2012

Mrna Granules And Ischemic Preconditioning

Michelle Rei Smith
Wayne State University,

Follow this and additional works at: http://digitalcommons.wayne.edu/oa_theses

mRNA GRANULES AND ISCHEMIC PRECONDITIONING

by

MICHELLE R. SMITH

THESIS

Submitted to the Graduate School

of Wayne State University,

Detroit, Michigan

in partial fulfillment of the requirements

for the degree of

MASTER OF SCIENCE

2012

MAJOR: Physiology

Approved by:

_____

Advisor   Date

DEDICATION

This thesis is dedicated to my support system. I would not have been able to navigate this journey without them.

To my amazing parents: Your unconditional love, support, and encouragement have always been my pillars of strength. My pursuit of a master's degree certainly would not have been possible without you. Thank you for always believing in me, even during times when I doubted myself.

To my sister Kim: You have always been an inspiration to me and a solid support in my life. Thank you for all your encouragement, words of wisdom, and most importantly, the comic relief to get me through those difficult times.

To Jay: Throughout the highs and lows of this program you made sure I never lost sight of my end goal. Thank you for always putting things into perspective and for occasionally reminding me to "chill out" because "everything will be okay".

the last two years.

TABLE OF CONTENTS

LIST OF TABLES

LIST OF FIGURES

LIST OF ABBREVIATIONS

1hR	1 hour Reperfusion
10I	10 minutes of ischemia + 1 hr reperfusion
2VO/HT	Bilateral Carotid Artery Occlusion Plus Hypotension
40S	Small Ribosomal Subunit
60S	Large Ribosomal Subunit
AA	Arachidonic Acid
AMPA	2-amino-3-(3-hydroxy-5-methylisoxazol-4-yl) propionate
ATP	Adenosine Triphosphate
CAr	Cardiac Arrest
CA/R	Cardiac Arrest and Resuscitation
CA1	Cornu Ammonis Region 1
CA3	Cornu Ammonis Region 3
CHX	Cycloheximide
COX-1	Cyclooxygenase 1
COX-2	Cyclooxygenase 2
CVA	Cerebrovascular Accident
DNA	Deoxyribonucleic Acid
DND	Delayed Neuronal Death
EAA	Excitatory Amino Acid
eIF2	Eukaryotic Initiation Factor 2
eIF2(αP)	Phosphorylated Form of eIF2α
eIF2α	Alpha Subunit on eIF2
eIF4	Eukaryotic Initiation Factor 4
ELAV	Embryonic Lethal Abnormal Vision
FISH	Fluorescent *In Situ* Hybridization
GDP	Guanosine Diphosphate
GEF	Guanine Nucleotide Exchange Factor
GTP	Guanosine Triphosphate
hr	hours
HSP	Heat Shock Protein
hsp70	70 kDa Heat Shock mRNA
HSP70	70 kDa Heat Shock Protein
I/R	Ischemia and Reperfusion
IF	Immunofluorescence
IPC	Ischemic Preconditioning
m^7G	7-Methyl Guanylyl Cap
MAP	Mean Arterial Pressure
MCAO	Middle Cerebral Artery Occlusion
MEF	Most Expressive Features
min	Minutes
mRNA	Messenger Ribonucleic Acid
mRNPs	Messenger Ribonucleoprotein Particles
NDS	Normal Donkey Serum
NIC	Non-Ischemic Controls
NMDA	N-methyl-D-aspartate

PABP	Poly-Adenylated Binding Protein
P-bodies	Processing bodies
PBS	Phosphate Buffered Saline
PCA	Principle Component Analysis
PFA	Paraformaldehyde
PIC	Pre-initiation Complex
PLA_2	Phospholipase A_2
poly-A	Poly-Adenylated mRNA
ROI	Region of Interest
ROS	Reactive Oxygen Species
sec	Seconds
SGs	Stress Granules
SSC	Saline-Sodium Citrate
TA	Texture Analysis
TA	Translation Arrest
tRNA	Transfer Ribonucleic Acid
TTP	Tristetraprolin
UTR	Untranslated Region
α	Alpha
β	Beta
γ	Gamma

CHAPTER 1

Background

1.1 Introduction to Brain Ischemia and Reperfusion Injury

1.1.1 Overview

The topic of my thesis pertains to brain ischemia and reperfusion (I/R) injury. The issue of brain I/R is a widespread problem that clinically manifests as either stroke or cardiac arrest and resuscitation. Furthermore, it has a major impact on the quality of life of the millions of individuals it afflicts each year, and costs billions of dollars in healthcare costs and lost productivity worldwide. While it is well understood that brain I/R results in neuronal death, the underlying mechanisms of exactly how these neurons die have continued to evade researchers and clinicians alike. As such, there has been almost complete failure of all clinical trials aimed to test potential therapeutics (O'Collins et al., 2006), and still to this date treatments available to prevent or halt the morbidity following the incidence of brain I/R are of very limited utility.

The work presented in this thesis is rooted in the translation arrest (TA) of protein synthesis and the ribonomic structures dictating this process as it occurs following brain I/R. The inhibition of protein synthesis is a reliable predictor of neuronal outcome: in neurons where protein synthesis is recovered, the cells will survive; if neuronal protein synthesis fails to recover, the cell will succumb to neuronal death. Data collected earlier in our lab has correlated this process of translation arrest to the presence of a specific, novel ribonomic structure known as mRNA granules. The aims of this thesis will be (1) to characterize the behavior of mRNA granules along a time course of ischemia and (2) study whether the protective phenomenon known as ischemic preconditioning (IPC) influences mRNA granules during early reperfusion I/R.

1.1.2 Two Types of Brain Ischemia: Global versus Focal Ischemia

Ischemia is a reduction or cessation of blood flow to an organ or tissue. Conversely, reperfusion is the subsequent restoration of blood flow. Both processes are capable of producing damage to the tissue, and each does so by different, yet synergizing, damage mechanisms. Furthermore, the various brain cell types are differentially affected, where some are able to overcome the damage and others succumb to it. There are two types of brain ischemia known as focal or global ischemia.

Focal brain ischemia occurs in a circumscribed brain area. The most significant clinical manifestation of focal ischemia is stroke. Occurrence of a stroke is marked by the reduction or complete elimination of blood supply to an isolated area of the brain. Often referred to as cerebrovascular accident (CVA), it is the third leading cause of death worldwide after heart disease and cancer, and remains the leading cause of adult disability. Tissue injury from focal ischemia follows a distinct pattern. There is a core region, which is at the epicenter of the occluded vessel; it consequently contains cells that die by necrosis. This core is surrounded by the penumbra region, consisting of a zone of hypoperfused cells (Muir et al., 2006). Cells in this region will die over the course of hours to days in a manner known as delayed neuronal death (DND).

Global brain ischemia on the other hand, is where the entire brain suffers from cessation of blood flow. Cardiac arrest is the most common clinical manifestation of global ischemia where there is complete cessation of the heart's mechanical activity and therefore absence of circulation (Roger et al., 2011). The pattern of damage following global ischemia is distinct from that of focal ischemia. In global ischemia, the patterns and morphological alterations are time dependent. For example, no obvious brain damage occurs following an ischemic duration of 4 minutes (min) or less. However,

widespread necrosis and brain death ensue if the global insult lasts 30 min or more. In the window of 4 to 30 min, specific neuronal populations begin to exhibit a gradient of ischemic impact (Hossmann and Kleihues, 1973). It has been established that the neurons most vulnerable to ischemia are the pyramidal neurons located in zone 1 of the Cornu Ammonis layer of the hippocampus (CA1), followed by CA3, then cerebral cortical layers II and III, cerebellar Purkinje cells, striatal and thalamic regions (White et. al., 1993), and then the remainder of the brain. These selectively vulnerable neurons go on to die within 24-72 hours (hr) following reperfusion via a process of DND, similar to the penumbra neurons of stroke. However, the more resistant vascular and glial cells survive the same insult as do the local interneurons (Kirino, 1982).

1.1.3 Clinical Manifestations and Relevant Statistics Concerning Global Brain Ischemia and Reperfusion

The incidence of sudden cardiac arrest within the population is significant: for adults forty years and older it is the leading cause of death (Roger et al., 2011). Out-of-hospital deaths caused by cardiac arrest claim the lives of an estimated 250,000 Americans each year (Forcina et al., 2009). The rate of patient survival following an in-hospital cardiac arrest is only 33% in children and 21% in adults (Roger et al., 2011). Even when individuals survive resuscitation, they are subject to serious brain damage if not already diagnosed as brain dead. It was found in a observational study that out of 1700 adults who met the criteria for having suffered an episode of primary cardiac arrest, only a dismal 1.4% of these patients remained neurologically intact (Eckstein et al., 2005). Moreover, out of the 70,000 individuals per year that survives cardiac arrest, only 3-10% of that population is able to maintain their quality of life. Another 60% of patients die after succumbing to extensive brain damage. Most survivors require

assistance to sustain a standard quality of life (Lloyd-Jones et al., 2009).

1.2 Mechanisms and Dynamic Changes Associated with Brain Ischemia/Reperfusion Injury

1.2.1 Consequences of Ischemia

The mechanisms of damage that arise during I/R have been extensively studied, and it is now well understood that these are a product of either the ischemic insult or the subsequent reperfusion. The brain heavily relies on a steady supply of oxygen and glucose to function properly. Thus when that supply is suddenly cut off, very serious consequences ensue. These encompass numerous, independently fatal pathways that ultimately result in neuronal death if the insult is extensive enough. This proposed "ischemic cascade" as it has been commonly referred to, is presented in Figure 1 (Lyden and Wahlgren, 2000).

At the onset of ischemia, the delivery of oxygen and glucose is eliminated completely (Krause et al., 1988).

Figure 1. An overview of the ischemic cascade. (Adapted from Lyden and Wahlgren, 2000).

Accompanying this loss is the rapid depletion of high energy phosphate stores within 3-4 minutes (Krause et al., 1988; White et al., 2000). The presence of adenosine triphosphate (ATP) is a requirement for maintaining neuronal ion gradients. Therefore, when ATP is depleted the ion gradients of sodium, potassium, and calcium quickly dissipate as the ions equilibrate across the neuronal membrane. The sudden influx of Na^+ and Ca^{2+} down their gradients into the cell triggers an overall membrane depolarization which fires action potentials and

releases glutamate into the synaptic cleft (Lyden and Wahlgren, 2000; White et al., 2000).

Excitotoxicity

The concept of excitotoxicity is based on the notion that the excessive release and activity of excitatory amino acids (EAAs) results in neuronal damage (Lyden and Wahlgren, 2000). Glutamate is the main excitatory amino acid transmitter in the brain. Under normal physiologic conditions it serves an important role in both metabolic and neurotransmitter functions, such as producing long-lasting changes in neuronal excitability and synaptic organization (Olney, 1990; Sattler and Tymianski, 2001). Glutamate acts via distinct subtypes of glutamate receptors, including the metabotropic receptors and ionotropic, ligand-gated ion channels such as N-methyl-D-aspartate (NMDA), kainate, and 2-amino-3-(3-hydroxy-5-methylisoxazol-4-yl) propionate (AMPA) receptors (Sattler and Tymianski, 2001). The physiologic binding of glutamate to the metabotropic receptors results in calcium release from intracellular stores. Ligand binding to NMDA receptors opens dual Na^+-Ca^{2+} channels, and binding to AMPA receptors opens Na^+ channels (Lyden and Wahlgren, 2000; White et al., 2000). Graded depolarization ultimately leads to the induction of action potentials and subsequent release of more glutamate (Danton and Dietrich, 2004). However under ischemic conditions, this well-balanced and highly regulated system becomes hyper-active and all the normal feedback is lost, driving the system into a deregulated state. The excessive stimulation of glutamate receptors plays a central role in mediating glutamate excitotoxicity and perpetuates the release of additional intracellular Ca^{2+} to further aggravate normal cell homeostasis. With the understanding of the ischemic cascade, research on pharmacologic agents such as NMDA and AMPA antagonists and

Ca^{2+} channel blockers have been pursued with only limited success in the clinic, mainly because of highly adverse side-effects due to glutamate antagonism in the brain (Danton and Dietrich, 2004).

Consequence of Ca^{2+} Imbalance and Influx

Calcium is a critical ion within cells, due to its key role as an intracellular messenger and modulator of various cellular processes (Martínez-Sánchez et al., 2004). As such, cells have an elaborate system of maintaining tight calcium homeostasis. Regulation is accomplished in three main ways: control of Ca^{2+} influx and efflux via the plasma membrane, shuttling into and out of intracellular stores, and buffering of intracellular Ca^{2+} (Martínez-Sánchez et al., 2004). These processes are directly and indirectly dependent on ATP, and consequently are forced into an unregulated state by ischemia. Such deregulation is central to activating a host of pathological processes. Both *in vitro* and *in vivo* studies (Siemkowicz and Hansen, 1981; Nakamura et al., 1999) have investigated the changes in intracellular calcium during ischemia. Siemkowicz and Hansen (Siemkowicz and Hansen, 1981) observed that in normoglycemic rats at the point of anoxic depolarization during global ischemia, the extracellular Ca^{2+} concentration sharply decreased from pre-ischemic normal levels of ~ 1.2 mM to ~0.1 mM within about 90 seconds following the induction of ischemia. In terms of the intracellular calcium, microelectrodes measured large increases in intracellular Ca^{2+} levels in both CA1 and CA3 hippocampal neurons (Silver and Erecińska, 1990). For instance, within the first minute of ischemia, small increases of 10-30 nM were observed. However by 2-3 minutes of ischemia, the level of cytosolic Ca^{2+} within the hippocampal CA1 neurons increased from 90 nM to 30 μM. Verification of these changes in calcium concentration was achieved with, MK-801, a non-

competitive antagonist of NMDA receptors. The effective blockade of NMDA receptors with MK-801 prevented the dramatic increase in intracellular Ca^{2+}, primarily seen in the hippocampus during ischemia, and it was concluded that this was due to the inhibition of Ca^{2+} channel opening and prevention of the subsequent Ca^{2+} influx (Silver and Erecińska, 1990).

Dramatically altered Ca^{2+} homeostasis during ischemia affects the cell's viability. For example, calpains are Ca^{2+}-dependent cysteine proteases consisting of μ-calpain and m-calpain, aptly named for the concentrations of calcium they require to become activated (micromolar and millimolar, respectively) (Goll et al., 2003). Calpains are known to play a role in synaptic remodeling. Specifically, the remodeling occurs in those cytoskeletal components attached to the plasma membrane which are active in the processes of cell motility and fusion (Goll et al., 2003). However during I/R, the calpains become hyper-activated and degrade the neuronal cytoskeleton. This has been shown in animal models of cerebral ischemia where MAP2 and α-spectrin, both integral cytoskeletal proteins, are degraded soon after the onset of ischemia, as evidenced by the presence of a 150 kDa α-spectrin fragment at 5 min and 60 min post-ischemia (Bartus et al., 1999; Neumar et al., 2001; Goll et al., 2003). Furthermore the administration of calpain inhibitors, AK-275 and AK-295, has been shown to prevent the calpain-induced spectrin breakdown observed in these earlier experiments (Bartus et al., 1999). Around the same time, Neumar et. al (2001) directly measured calpain activation in neurons following both global and focal ischemia and also showed two important regulators of protein synthesis were degraded by calpain, eIF-4G and eIF4E (DeGracia, 2004). These are two important eukaryotic initiation factors essential to the process of protein synthesis initiation and will be discussed below.

Another important calcium dependent process affected by ischemia deregulation is calcium-regulated phospholipases; specifically phospholipase A_2 (PLA_2). The phospholipases are an important class of enzymes that are responsible for catalyzing the cleavage of fatty acids from phospholipids (Sun et al., 2004). PLA_2 is the enzyme responsible for releasing free fatty acids via the hydrolysis of the *sn*-2 fatty acyl bond and ultimately for the generation of arachidonic acids (AA) leading to the production of eicosanoids (Dennis, 1994). Under physiologic conditions, PLA_2 participates in the inflammatory process by releasing the arachidonic acid which in turn serves as a substrate for cyclooxygenase 1 and 2 (COX-1, COX-2) which ultimately produce the prostaglandins (Cummings et al., 2000). PLA_2 also contributes to other processes of the cell including signal transduction and host defense.

During brain ischemia, hyperactivation of PLA_2 alters permeability of the membranes (Murakami et al., 1997) and generates high levels of arachidonate (Bazan, 1989). The production of prostanoids, downstream products of arachidonate metabolism, is a well-known biochemical marker associated with ischemia and other CNS disorders (Sairanen, 1998). Prostanoid production, catalyzed by the conversion of arachidonic acid via cyclooxygenases, contributes to the deleterious production of reactive oxygen species (Sairanen et al., 1998). In studies performed by Sairanen et. al (1998), they observed that following focal ischemia there was prominent COX-2 induction in the neurons located at the site of the infarct core. Taken together with the notion that prostanoid production and free radicals can exacerbate tissue damage during episodes of cerebral ischemia, it suggests that COX-2 activity plays a crucial role in the overall process of excitotoxicity.

The disrupted state of calcium regulation is an important underlying similarity in

the above examples of biochemical disturbances during ischemia. However, the damaging effects of ischemia are only part of the story.

1.2.2 Consequences of Reperfusion

Reperfusion is the resumption of blood flow after ischemia, allowing metabolites and nutrients to be restored to the tissue. The restoration of blood and oxygen to the tissues is necessary to prevent the immediate death of cells, however, in a paradoxical fashion, this restorative act is fundamentally harmful to tissues and perpetuates the damage incurred during the ischemic period.

As blood flow is restored to the ischemic tissue, it is reintroduced into an altered cellular environment. It is due to the damage products accumulated during ischemia and their reaction with oxygen that makes reperfusion a double-edged sword. In the initial period of reperfusion, the buildup of vasodilating metabolites during the ischemic period now produce an increase in blood flow (hyperemia) and the levels of ATP are restored within the first 10 min (Krause et al., 1988). In the presence of ATP, ion-gradients are re-established after 20 min of reperfusion (Hoehner et al., 1987). Hyperemia is short lived however, as by 60 min of reperfusion a hypoperfusion occurs (Krause et al., 1988). At this point since the metabolic demands of the brain are still very high, there is an uncoupling of blood flow with the brain's metabolic needs during the reperfusion period, and this results in at least a 50% depression of the metabolic rate over the course of 6 hours following the ischemic event (Mies et al., 1990). Furthermore, the release of various factors such as reactive oxygen species and lipid peroxidation products further exacerbates cell damage. Additionally, pathways involved in cell signaling are altered and there are major changes in the protein synthesis system during reperfusion.

Reactive Oxygen Species

The presence of oxygen during reperfusion generates reactive oxygen species (ROS) (McCord, 1993). The presence of ROS is detrimental to the cell. As mentioned earlier, arachidonic acid is released by PLA$_2$ during ischemia. During reperfusion, arachidonate is catalyzed by cyclooxygenase into prostaglandin G, and ultimately prostaglandin H and a free radical (Krause et al., 1988). In the oxidative degradation which occurs next, the resulting free radicals strip the phospholipid membrane of its free electrons thus affecting the membrane properties of permeability and fluidity (Farber, 1982). This process of lipid peroxidation is equally harmful to the cell as it results in the cross-linking of fatty acid side chains and polymerization of membrane lipids (Freeman and Crapo, 1982) and leads to inhibition of the Na$^+$-K$^+$ ATPase (Demopoulos et al., 1980).

Dysfunction at the level of Protein Translation: Translation Arrest

Another major change in reperfusion is the focus of this thesis. It was first reported in 1971 (Kleihues and Hossmann, 1971) that translation of proteins is inhibited during reperfusion. We will refer to protein synthesis inhibition by the term "translation arrest" (TA). They observed: (1) the amount of incorporated radioactive leucine decreased in *in vitro* translation of brain homogenates exposed to 30 min reperfusion compared to controls, and (2) polysomes disaggregated during reperfusion as visualized with an electron microscope and through biochemical quantification using polysome profiles.

However, TA was not present in *in vitro* translation reactions derived from brain that underwent only ischemia but not reperfusion. They showed that during the ischemic period, messenger ribonucleic acid (mRNA) remains attached to the

ribosomes, and suggested that polyribosomes "freeze" due to the complete lack of energy producing metabolism during ischemia. This halts protein synthesis solely due to lack of metabolic energy during the ischemic period.

However, that polyribosomes dissociated following reperfusion, even after ATP levels returned, suggested that TA during reperfusion was in some way linked to the inhibition of translation initiation (Kleihues and Hossmann, 1971). Even in 1971 it was understood that polysomes disaggregated because they could not re-initiate; and this notion was clear even though all the molecular details were not yet known at the time.

Thereafter, many labs confirmed the findings in this initial study by showing that indeed for several hours following reperfusion, protein synthesis is inhibited (DeGracia, 2004). This was ultimately elaborated upon and gave way to yet another significant discovery: that the recovery from TA is different depending on the brain region, and correlated with the survival of a particular region. When a brain region recovers from TA it will survive, whereas the vulnerable
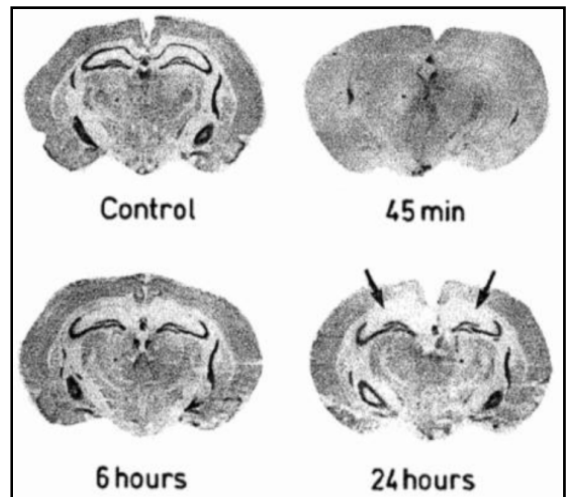
Figure 2. Autoradiographs showing failed recovery of translation. Arrows indicate lack of radioactive amino acid incorporation into the CA1 region following 5 min global ischemia and 24 hr reperfusion (Hossmann, 1993).

brain regions fail to recover from TA and consequently succumb to DND (Hossmann, 1993).

Figure 2 documents this occurrence via a series of autoradiograph images showing *in vivo* protein translation following global brain I/R in gerbils. The main area of interest, the hippocampus, is shown following 5 min global ischemia and subsequent

periods of reperfusion up to 24 hr. The results illustrate that translation is completely inhibited in all brain regions following 5 min ischemia, 45 min reperfusion. By 6 hr of reperfusion, there is recovery of translation within all areas of the hippocampus except for the hippocampal CA1 neurons, demonstrated by lack of ^{14}C-leucine incorporation. Lack of protein translation in CA1 persisted throughout 24 hr reperfusion, and invariably the CA1 cells died by 72 hr reperfusion (Hossmann, 1993).

This observation firmly linked DND following I/R to TA, and it brought TA to the forefront of explanations for why DND occurs in some brain regions but not others following reperfusion. It became essential to investigate every aspect of the translation process in order to understand and pinpoint the exact step(s) that goes awry during I/R, which in turn results in the DND of vulnerable neurons following reperfusion.

1.3 Consequences of Reperfusion on Overall Protein Synthesis

1.3.1 Overview of Protein Synthesis: Initiation, Elongation, Termination

Protein synthesis is a well-understood process consisting of three main phases: initiation, elongation, and termination. Translation initiation uses multiple eukaryotic initiation factors (eIF) that facilitate the assembly of mRNA, 40S and 60S ribosomal subunits and a special transfer ribonucleic acid (tRNA) known as methionine-
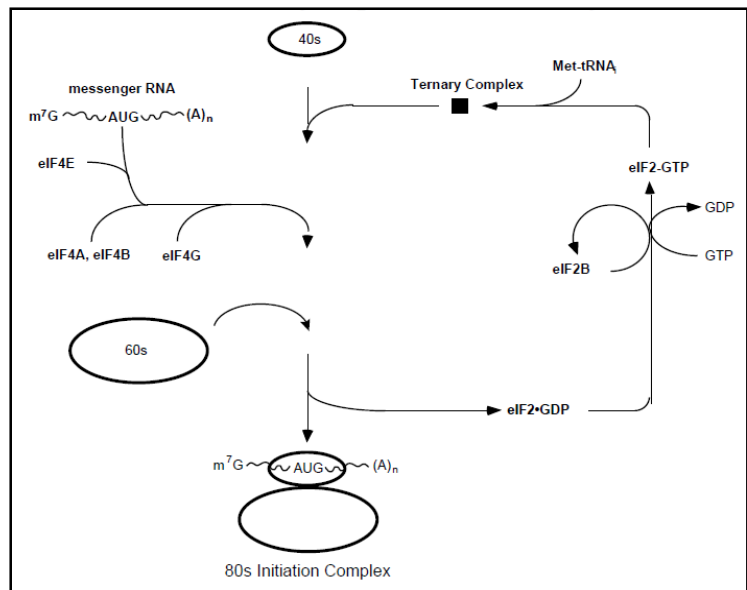
Figure 3. Overview of steps in the initiation phase of translation.

conjugated initiator tRNA, denoted as tRNA$^{MET}_i$. Once the 80S ribosomal complex is

formed, as shown in Figure 3, the elongation phase begins and additional factors facilitate the movement of the ribosome along the mRNA, adding a specific amino acid as dictated by a triplet codon. The elongation process continues in the 5' to 3' direction, adding amino acids to the growing polypeptide chain. This process continues until the ribosome encounters a stop codon on the mRNA, which signals the end of elongation and the beginning of termination. The newly synthesized protein is also subject to a series of posttranslational events, such as protein folding and chemical modifications, which ultimately transform the new polypeptide chain into a functional protein correctly folded into its three dimensional conformation.

Each of these phases are subject to regulation in order to control the overall level of protein being synthesized within a cell. However, the regulation of initiation is the most important because it is the rate limiting step in protein synthesis, and it selects which mRNAs will be translated at any given moment.

1.3.2 Rate-Limiting Steps: Translation Initiation Factors

Two specific proteins control the rate limiting steps of translation initiation, and these are subject to specific regulation. The proteins are known as eukaryotic initiation factor 2 (eIF2) and eukaryotic initiation factor 4 (eIF4), mediate the two rate limiting steps in the overall process of translation initiation (Merrick, 1990). The role of eIF2 is to catalyze the delivery of the methionyl-charged $tRNA_i$ to form the 43S pre-initiation complex (PIC). Regulation of this step allows the cell to control the global rate of total protein synthesis. The absence of the first amino acid $tRNA_i$ at the P site prevents protein synthesis from taking place. The second rate limiting step is eIF4 delivering the mRNA to the 43S PIC. Regulation of this step provides the cell's ability to control how much of, and which mRNAs will be translated. Given their central roles in the process

of initiation, it is essential to understand what factors and conditions can alter the regulation of these two necessary players which ultimately determine the direction of protein synthesis.

Role of eIF4F in Regulating Translation Initiation

eIF4F is a hetrotetramer that consists of the following subunits: eIF4A, eIF4B, eIF4E, and eIF4G. The function of this tetrameric structure is to deliver the mRNA to the 43S PIC and for that reason is regarded as one of the rate limiting steps of translation initiation. Each subunit serves a distinct role in uniting the mRNA with the ribosome. eIF4A is an ATP-dependent RNA helicase that, along with the eIF4B cofactor, facilitates the unwinding of the mRNA's secondary structure in the 5' untranslated region (UTR) and promotes the movement of the ribosome in the 5' to 3' direction (Gingras et al., 1999; Sonenberg and Dever, 2003). This unwinding step enables the process of scanning, the translocation of the PIC along the mRNA in the 5' to 3' direction, which allows the ribosome to locate the start codon. eIF4E is the cap binding protein which binds the 7-methyl guanylyl cap (m^7G) at the 5'end of the mRNA. Its presence is absolutely essential to the translation of all capped mRNA (Gingras et al., 1999) and is subject to tight regulation (discussed below).   eIF4G is a large scaffold protein that participates in a ribosome-mRNA
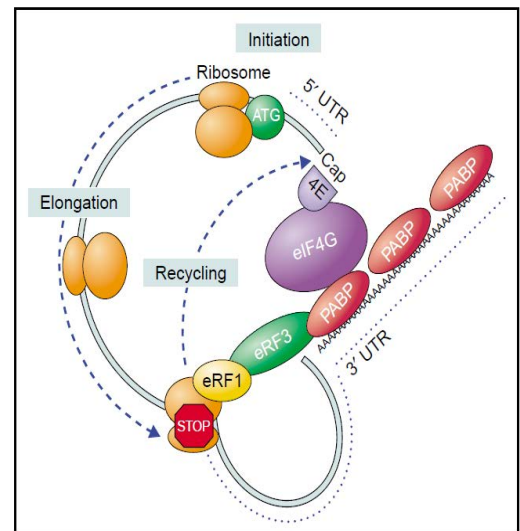
Figure 4. An illustration of the circularization of mRNA mediated by eIF4. (from Sonnenberg and Dever, 2003).

bridging function, and also contains sites for binding eIF4E, eIF4A, eIF3, and poly-A binding protein (PABP), and several other proteins (Gingras et al., 1999).   This

association between PABP with eIF4G is responsible for the circularization of mRNA, shown in Figure 4. Note how eIF4E is bound to eIF4G, while on another portion of eIF4G, it binds PABP, the latter bound to the 3' polyadenylated (pA) tail. The significance of this circularization is to produce a synergistic interaction between the 5' cap and the 3'poly-A tail which makes initiation more efficient (Sonenberg and Dever, 2003). Given the importance of eIF4E and eIF4G, their tight regulation is what allows the cell to dictate the selectivity of mRNAs that get delivered to the ribosome for translation.

Role of eIF2 in Regulating Translation Initiation

eIF2 has a trimeric structure comprised of three subunits: alpha (α), beta (β), and gamma (γ). The beta and gamma subunits are necessary for binding the tRNA and GTP, and the alpha subunit is the regulatory subunit. In order to understand the regulation of eIF2 conferred by the alpha subunit, it is important to first establish the underlying mechanism of eIF2 function. eIF2 is a G-protein, meaning that in order to be active, it must bind GTP. At the start of initiation, eIF2 complexes with GTP and then becomes capable of binding Met-tRNA$_i$. Upon binding, the ternary complex is formed, which consists of eIF2-GTP-Met-tRNA$_i$ (DeGracia et al., 2002). Together, this ternary complex then binds with the small 40S ribosomal subunit to form the 43S PIC. The 5'end of the mRNA recruits eIF4F coupling it to the 43S PIC, thus forming the 48S PIC. Now the process of scanning can proceed in the 5' to 3' direction until the AUG start codon is encountered. As soon as this happens, scanning ceases. Hydrolysis of the GTP then occurs by the base pairing between the Met-tRNA$_i$ anti-codon and the AUG start codon (Sonenberg and Dever, 2003). The hydrolysis step converts GTP in the ternary complex to GDP. Consequently, this event leaves the eIF2 bound to GDP and

releases it along with the other initiation factors from the 48S PIC. The large 60S ribosomal subunit is now able to access and bind the 48S PIC, allowing formation of the translation-competent 80S complex and signaling the end of the initiation process (Sonenberg and Dever, 2003).

eIF2 requires the binding of GTP to be active. eIF2 is unable to bind the Met-tRNA$_i$ when it is not bound to GTP. However, after initiation, the GTP is hydrolyzed and leaves eIF2 bound to GDP. In order for eIF2 to recycle and function in subsequent rounds of initiation, the GDP must be replaced with GTP. This step is carried out by the enzymatic activity of another eukaryotic initiation factor known as eIF2B (also called guanine nucleotide exchange factor, GEF), whose function is to replace the GDP with a GTP, thus regenerating the eIF2-GTP complex. As such, eIF2B is a necessary component to maintain translation initiation. If there is an insufficient amount of eIF2B present, the initiation step and subsequently translation as a whole will either be slowed or stopped. The stoichiometric ratio of eIF2 to eIF2B in most cells is 5:1 (Oldfield et al., 1994) which is an important fact in the regulation of initiation.

The regulation eIF2B, the activity of eIF2, the rate of initiation, and ultimately the overall rate of translation all hinge on one event: the phosphorylation of the alpha subunit on eIF2 (eIF2α). The alpha subunit is the regulatory component of eIF2 because it is a substrate for phosphorylation on the serine 51 residue, denoted as eIF2(αP). When this occurs, the binding affinity between eIF2(αP) and eIF2B increases 150-fold in comparison to the alpha-unphosphorylated form eIF2 (Rowlands et al., 1988). This means that eIF2B becomes bound so tightly to eIF2(αP) that it is unavailable to interact with its normal substrate eIF2-GDP and therefore is unable to perform the necessary enzymatic exchange of GTP for GDP. In other words, eIF2 is

normally a substrate of eIF2B, but when eIF2α is phosphorylated, it converts eIF2 into a competitive inhibitor of eIF2B. Thus, eIF2-GDP will accumulate, and the pool of eIF2-GTP needed to form the ternary complex becomes depleted so delivery of the tRNA$_i^{MET}$ to the 40S subunit slows or halts. If enough eIF2B is sequestered by eIF2(αP), then initiation of translation is halted, and protein synthesis also grinds to a halt. The aforementioned concentration 5:1 of eIF2:eIF2B means that if only 1 out of 5 (20%) of eIF2 becomes phosphorylated, that will be sufficient to competitively inhibit all eIF2B, thus resulting in complete translation arrest (Burda et al., 1994; Oldfield et al., 1994).

1.3.3 The Role of Reperfusion in Altering Translation Initiation

The changes evoked in the rate limiting eukaryotic initiation factors, eIF2 and eIF4, during reperfusion have been thoroughly investigated. In the first such study, Hu and Wieloch (1993) measured the activity of eIF2β following global cerebral ischemia. They concluded that following 15 minutes ischemia and either 30 minutes or 1 hour reperfusion, the ternary complex was inhibited, but could be restored upon addition of purified eIF2β. Therefore, this suggested eIF2B inhibition during reperfusion caused inhibition of protein translation (Hu and Wieloch, 1993). Subsequently, Burda et. al (1994), presented evidence that following brain I/R, levels of eIF2(αP) were substantially increased, thus concluding that it was this phosphorylation event of eIF2α that impaired eIF2B activity, prevented formation of the ternary complex, and led to the inhibition of translation initiation (Burda et al., 1994). Burda's results were confirmed by DeGracia et. al (1996), who showed 30% of eIF2α was phosphorylated. Subsequently, DeGracia et. al (1997) developed the first phosphor-specific antibody against serine 51 phosphorylated eIF2α, which made it possible to map by immunohistochemistry the distribution of eIF2(αP) in the reperfused brain. Their results presented a clear picture

that first of all, eIF2(αP) was present in all post-ischemic neurons, and secondly, that eIF2α phosphorylation peaked at 10 minutes but began to decline by 4 hours of reperfusion to baseline levels (Kumar et al., 2003). These studies solidified the understanding that the phosphorylation of eIF2(α), which thereby resulted in translation arrest, was a transient event and therefore was not linked to cell death.

In terms of the changes occurring with eIF4F during reperfusion, Dr. DeGracia was the first to show degradation of the scaffold protein eIF4G, but no change in eIF4E following brain I/R (DeGracia et al., 1996). Burda and colleagues later confirmed this observation and additionally, they localized the highest level of eIF4G degradation to the hippocampal CA1 neurons (Martín de la Vega et al., 2001). Furthermore, it was shown that the loss of eIF4G was caused by μ-calpain during reperfusion (Neumar et al., 1998) and (García et al., 2004) later confirmed this finding.

The end conclusion from these studies has remained evident: changes in initiation factors share a commonality of transient alteration during the first several hours of reperfusion, but however eventually return to basal state whether in the vulnerable or resistant neuronal populations. This provides strong evidence that transient changes in eIFs do not have a direct correlation and impact on the pattern of cell death as observed in vulnerable neurons that eventually go on to die by DND.

1.4 The Ribonomic Network and mRNA Regulation

1.4.1 Stress Granules, HuR Granules, and other Ribonomic Structures

Turning the focus now to additional regulatory processes that may contribute to sustained TA, I will briefly discuss a variety of structures that have been proposed to play a role in executing these changes in the post-ischemic brain. It has been proposed in the DeGracia laboratory (DeGracia et al., 2002) as well as other laboratories

(Paschen, 1996; Martín de la Vega et al., 2001) that a strong correlation exists between TA in the post-ischemic brain and the intracellular stress responses induced by I/R. Specifically, stress responses such as the heat shock response and unfolded protein response are well-known to cause TA. However, once the stress responses have been successfully carried out, normal translation recovers. This pattern is what is observed in resistant neurons. But TA persists in vulnerable neurons and is correlated with the lack of successful stress response execution. Therefore, there is some type of important connection between TA and stress responses.

The field of ribonomics, the study of how mRNA molecules are regulated by mRNA binding proteins, has clarified the understanding of mRNA regulation (Tenenbaum et al., 2002) and has provided an expanded perspective from which to think about the role of TA and I/R-induced stress responses. Central to the understanding of ribonomics is the notion that mRNA molecules are dynamically regulated and mRNA activity involves much more than simply moving from nucleus to ribosomes as it gets translated into protein. In fact contrary to this understanding, mRNA molecules are bound to a variety of proteins, throughout its life cycle and form complexes known as messenger ribonucleoprotein particles (mRNPs) (Anderson and Kedersha, 2006). There have been at least a dozen of these particles identified within recent years, and nine of these known foci are depicted in Figure 5. Each mRNP maintains a unique, yet integrated function in regulating the flow of the cell's mRNA from biogenesis to degradation (DeGracia et al., 2008). All of these subcellular structures taken together comprise the ribonomic network. The mRNA functions carried out by this network include: transcription, processing, routing/transport, silencing/storage, translation, and degradation (DeGracia et al., 2008). Thus, a firm

understanding of each of these ribonomic structures and their functions is essential to understanding the regulation of mRNA during physiologic and stress conditions.

mRNA Handling outside the Nucleus

Because we are focused on cytoplasmic mRNA regulation, I will not describe nuclear mRNA processing here. Following transcription and processing in the nucleus, the mRNA gets routed to the cytoplasm. Based on the needs and conditions of the cell at a particular time, mRNA is shuttled to any one of the mRNPs, discussed below.
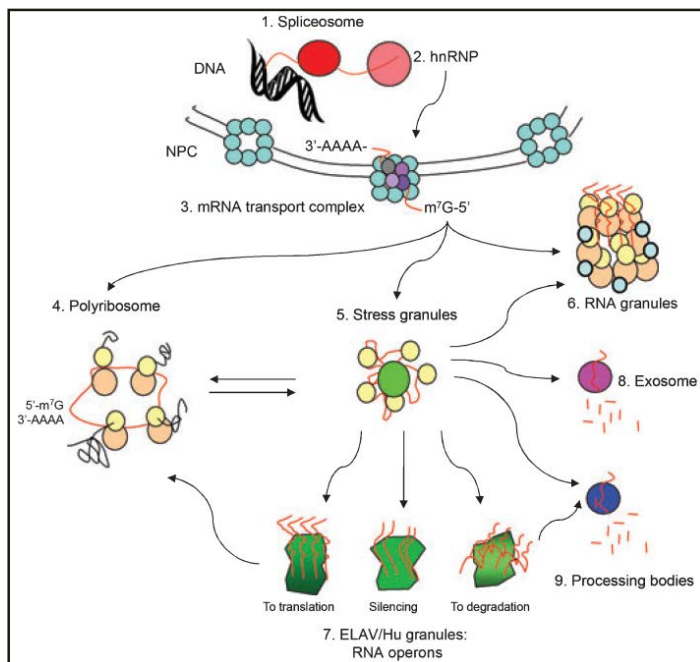
Figure 5. Depiction of structures that comprise the ribonomic network. (from DeGracia et. al, 2008).

Stress Granules

In the context of environmental stressors, cells maintain the ability to reprogram their translation machinery in order to selectively translate the proteins necessary to combat the stressor (Kedersha et al., 2005). When this occurs, the translation of the normal mRNAs being translated in the cell must stop and be removed from the polysomes in order to make ribosomes available for the translation of stress-induced mRNAs. The changing of the mRNA population on the ribosomes directly correlates

with the stress-induced TA (Kedersha et al., 2005). However, the normal, pre-existing transcripts prior to the stress must be dealt with and contained. The work of Anderson and Kedersha (2005) has revealed that the role of stress granules (SGs) is to serve as sites of "mRNA triage" where mRNAs from the disaggregated polysomes first accumulate and then are routed to the other ribonomic foci where they will either be reinitiated, degraded, or stored (Kedersha et al., 2005).

Polyribosomes

It has been known for a long time that polysomes are the subcellular structures that catalyze the conversion of the mRNA genetic information into protein. Recently however, the original dogma, in which mRNA goes immediately to ribosomes to become translated, has been challenged in light of the concept of the ribonomic network. Anderson and Kedersha (Anderson and Kedersha, 2006) maintain that polyribosomes are subject to formation and disaggregation just like the other mRNPs in order to meet the needs of the cell. The transient nature of polysomes, as a function of a cell's physiological or pathological condition, is related to qualitative mRNA regulation, whereby the ability of specific mRNAs to access the ribosomes will ultimately determine the cell's proteome and effectively its phenotype (DeGracia et al., 2008).

ELAV/HuR Granules

The embryonic lethal abnormal vision (ELAV) is the Drosophila homolog of the mammalian Hu proteins which play a critical role in mRNA regulation. HuR has long been known to stabilize mRNAs that contain a specific sequence in the 3' untranslated region (3' UTR) known as an adenine and uridine rich element (ARE). More recently, the laboratory of Jack Keene has determined that Hu proteins play a larger role in cell function by participating in molecular complexes that partition mRNAs into sets or

cohorts based on functional or structural similarities. This partitioning feature provides for the coordinated handling of mRNAs and has been referred to as an 'RNA operon' (Keene, 2007). Bacterial operons are sets of functionally related genes that are simultaneously transcribed and translated. The coordinated handling of eukaryotic mRNAs is functionally similar and therefore Keene uses the term 'RNA operon'. The HuR granules act as RNA operons to coordinate mRNA cohort activity, specifically to target them for collective translation, silencing, or degradation (DeGracia et al., 2008). These HuR granules are believed to provide the basis for the cell to execute complex physiologic "programs" of activity like stress responses and differentiation. This operon-like feature provides the eukaryotic cell with a level of speed, efficiency, and flexibility in genetic reprogramming to respond to changes in the cell's environment. The cell cannot solely rely on transcriptional regulation because large scale changes in gene expression require hours, and is often too slow for many important biological processes, such as, for example, ischemic injury or heat shock (Keene, 2007).

Processing Bodies and Exosomes

These are the important mRNP structures responsible for the degradation of mRNA (DeGracia et al., 2008). Processing bodies (P-bodies) possess both exonucleolytic and RNA silencing machinery, and therefore maintain the ability to either silence or degrade the mRNA (Brengues et al., 2005). On the other hand, exosomes possess the 3'-5' exonuclease machinery necessary to decap and deadenylate the mRNA which are enzymatic prerequisites for mRNA degradation (Schwartz and Parker, 2000). mRNA degradation serves as an important pathway for mRNA regulation as it maintains the half-lives of transcripts (DeGracia et al., 2008).

1.4.2 Ribonomics and Post-Ischemic Translation Arrest

As introduced earlier, the role of SGs is to act as a triage center for the mRNA. In the work performed in support of his Ph.D. dissertation, Dr. Foaz Kayali, working in the DeGracia laboratory, proposed that SGs played a key mechanistic role in the prolonged translation arrest observed in post-ischemic CA1 neurons that would eventually go on to die. He hypothesized that following I/R, SGs would form in all post-ischemic neurons and furthermore, it was the prolonged presence of these SGs during reperfusion that caused the irreversible TA seen in CA1 neurons. Additionally, he hypothesized that the SGs formed in CA1 must be different from those observed in CA3. In order to test these hypotheses, global ischemia was induced in the rat using a cardiac arrest and resuscitation (CA/R) model. Overall Dr. Kayali's work was significant in providing the first *in vivo* account of the behavior of SGs in any whole animal model, and specifically during the first 4 hours of reperfusion following 10 minutes of global ischemia.

His results revealed that the 40S ribosomal subunit (visualized with anti-small ribosomal protein S6 antibody) was completely sequestered (colocalized) within SGs (which were detected using anti-TIA-1 antibody) during a critical period in which eIF2α(P) was in a dephosphorylated state 80% from its peak phosphorylation (Kayali et al., 2005). This was an important finding which related a mechanism, the sequestration of the small 40S ribosomal subunit, to the prolonged translation arrest seen in CA1 neurons, supporting a plausible connection between prolonged TA and DND. In a subsequent study, DeGracia et al. (2006) immunomapped eIF4G, again using the CA/R model, in order to clarify what role the degradation of eIF4G had on reperfusion-induced neuronal death. It was observed that when eIF4G and TIA-1 were co-stained, the

eIF4G formed granules in the CA1 neurons at 90 min and 4 hr reperfusion, which suggested that 4G fragments were accumulating in nonproductive complexes, thus contributing to the prolonged TA (DeGracia et al., 2006).

As important as these findings were, there was a major limitation in the model which ultimately prevented extensive investigation into the extended reperfusion time points. The CA/R model was limiting in the fact that reperfusion could only be carried out to 4 hr because the animal model is so lethal to the experimental animals. Yet DND occurs at 72 hr reperfusion. The CA/R model yields a low survival rate of < 25% and the animals die more frequently as the duration of reperfusion is increased (Montie et al., 2005). Furthermore, the CA/R model damages not only the brain, but also peripherally the heart, lungs, kidneys, and GI tract (Montie et al., 2005). Given these limitations, the DeGracia laboratory adopted a different model of inducing global ischemia known as the bilateral carotid artery (two-vessel) occlusion plus hypotension ischemia model (2VO/HT). As documented by (Smith et al., 1984), the 2VO/HT model generates DND but maintains a much higher survival rate of 85%, and the animals can be reperfused for essentially any duration of time, as opposed to being limited to 4 hours.

The application of this superior model of global brain ischemia, the 2VO/HT model, made it possible to assess the behavior of SGs out to later reperfusion time points. In a 2007 study, the model was used to induce 10 min global ischemia in the rat, followed by 1, 2, and 3 days reperfusion (DeGracia et al., 2007). The results of this study demonstrated that out to a period of 48 hr reperfusion, the levels of TIA-1, the marker for SGs, did not change in either cytoplasmic or nuclear fractions taken from CA1 and CA3 neurons. Furthermore, the levels of S6 did not decrease in CA1.

Comparison of data using the two different models of brain ischemia highlighted significant discrepancies in the cardiac arrest results. The 2VO/HT model of ischemia showed no significant change in SGs out to 48 hr of reperfusion. Thus, the result of 40S subunits sequestered into SGs seen in the cardiac arrest model did not hold in the 2VO/HT model. But the 2VO/HT model causes DND of hippocampal CA1 neurons. Therefore, the conclusion was that the changes seen in the first 4 hr of reperfusion after cardiac arrest were not necessary to cause DND. While this provided greater insight about the role of SGs in post-ischemic stress response, it failed to answer the question of what caused prolonged TA in neurons that would eventually die by DND.

The next major project was conducted by Dr. Jill Jamison, another former Ph.D. student in the DeGracia laboratory. Dr. Jamison studied the microscopic appearance and colocalization properties of total mRNA in reperfused neurons using the 2VO/HT model. She used the method of fluorescence *in situ* hybridization (FISH) which is also the main technique of my work in this thesis. The application of the FISH technique, based on the protocol used in Bessert and Skoff (Bessert and Skoff, 1999), allows for the visualization of all polyadenylated mRNAs by hybridizing a 5'-biotinylated 50-mer oligo-dT probe.

Her main finding was that she observed a redistribution of cytoplasmic poly(A) mRNAs that went from a homogenous staining pattern in the cytoplasm of control neurons, to a highly granular appearance in reperfused neurons. The granulated appearance of poly-A mRNAs was termed by the lab "mRNA granules". The mRNA granules were observed to be reversible in CA3 but irreversible in CA1 over the 48 hr time course of reperfusion studied. Most significantly, when radioactive amino acids were administered IV to the animals and proteins were isolated and measured for

radioactive incorporation, it was found that whenever protein synthesis rates were below the control level, the cells also possessed mRNA granules. There was a strict correlation between *in vivo* protein synthesis and mRNA granules. Further colocalization studies shed light on this correlation.

The colocalization of mRNA granules with various mRNA binding proteins was undertaken. The proteins studied were: eIF4G, HuR, poly-A binding protein (PABP), S6, TIA-1, and tristetraprolin (TTP; a marker for processing bodies). mRNA granules did not colocalize with TIA-1, or TTP, which indicated they were independent entities from both SGs and processing bodies. A more complicated result occurred when HuR was studied. There were differences in HuR colocalization between resistant CA3 and vulnerable CA1 neurons. The colocalization of HuR and poly-A occurred early on in CA3, beginning at 1 hr reperfusion. In CA1 neurons HuR/mRNA granule colocalization was not observed until 36 hr reperfusion (Jamison et al., 2008). Moreover, it was observed that when HuR colocalized with mRNA granules, this correlated with the translation of stress-induced 70kDa heat shock protein (HSP70) (Jamison et al., 2008).

It was probably the most important finding of the colocalization studies that poly-A mRNA granules did not colocalize with the 40S marker, S6. This indicated that mRNA was physically separated from the 40S subunits, and gave a clear cut explanation for the correlation between mRNA granules and decreased protein synthesis in the reperfused neurons. The mRNA granules were some type of subcellular structure that partitioned mRNA away from the 40S subunit, and this would therefore prevent translation. In a study more recently conducted in the lab, Dr. Jamison showed that mRNA granules also did not colocalize with a marker of the 60S subunit (Jamison et al., 2011), indicating that the mRNA granules were separated from

both ribosomal subunits. This is a highly significant finding and is the first demonstration of any mechanism at all that strictly correlates a structural change in the translation machinery with the TA that occurs in reperfused neurons.

1.4.3 Technical Issues of Studying mRNA Granules in Microscope Images

Since the identification of mRNA granules, a tremendous amount of work has been done in Dr. DeGracia's lab to further characterize them in terms of how and when they form in the context of global brain I/R. Given the microscope intensive nature of visualizing and studying these granules, a method needed to be developed that would allow for the objective quantification of the appearance of poly-A staining in the microscopy data. In a recent study, a method known as **texture analysis** was employed as a means to quantitatively analyze subcellular morphological changes as obtained from the microscope images (Szymanski et al., 2012). Given that mRNA granules introduce a significant change to the texture of the neuronal cytoplasm, this provided an ideal situation for the implementation of the texture analysis techniques. Equipped with this technique, they could then more accurately quantify the data obtained by carrying out various manipulations on the mRNA granules.

Texture analysis is a computer-based method to quantify differences in images. The overall process of texture analysis will be described in greater detail in the methods section, but essentially it utilizes a program known as MaZda to define an image in terms of its multiple texture features which are assigned as numerical values. By way of these numerical values, the program is then able to extract subtle details contained within microscopy data in an organized and consistent manner. In terms of real life applications, it is used in the fields of artificial vision, used by the military to study satellite images, and it is used in biomedicine to diagnose MRI images, for example, to

diagnose the presence of brain tumors (Zook and Iftekharuddin, 2005). It has also been used previously to characterize changes in microscope images of cells. The technique involves masking off a region of interest (ROI) and then calculating a number of different parameters that characterize the pixels in the ROI. The texture analysis used by our lab calculates 168 different texture features. For example, the variance of the pixels from the mean intensity is one such parameter. The variance in pixels that surround a given pixel is another measure.

In the Szymanski et al. (2012) study they applied the use of a pharmacological agent in order to better understand the molecular biology of mRNA granules. Cycloheximide (CHX) is a well-known glutarimide antibiotic that inhibits protein synthesis by effectively "freezing" the polysomes in an inactive state (Pestka, 1971). More specifically, it halts elongation by preventing the deacylated tRNA from being released by the ribosome, thus preventing the disassembly of polysomes (Pestka, 1971). The results of this study showed that when CHX was administered via intraperitoneal (I.P.) injection 15 min prior to 10 min ischemia, it inhibited the formation of mRNA granules. However, if CHX was given after 10 min ischemia at 15 min reperfusion there was no effect, and the texture parameters calculated from microscope images were indistinguishable from vehicle treated reperfused samples (Szymanski et al., 2012). Since the primary action of CHX is to prevent the dissociation of polyribosomes, these results indicated that the formation of the mRNA granules is dependent upon the liberation of polysome-bound mRNAs via polysome dissociation, and consequently this dissociation must be an upstream event to the formation of mRNA granules. In addition, this study was valuable for demonstrating that CHX can be used as an experimental tool to modulate mRNA granules. I will use CHX in this

fashion in the studies described ahead.

1.5 Neuroprotection and Ischemic Preconditioning

1.5.1 The Concept of Neuroprotection

Up to this point, I have reviewed studies that first identified the correlation between TA and DND. I next detailed studies which led to our current understanding of the changes in the translational system by brain I/R, and how mRNA granules provide the first mechanism that correlates perfectly with TA in reperfused neurons. I will now shift gears to discuss a topic important in the field of brain I/R, and that is the phenomenon of ischemic preconditioning (IPC). This understanding of IPC is significant because I will propose to study how mRNA granules behave following IPC.

The concept of IPC is centered on the understanding that a very brief ischemic event which in itself is nonlethal, can induce tolerance within a tissue and confer resistance or protection to the cell against cell death during a subsequent, normally lethal ischemic insult (Barone et al., 1998; Wiegand et al., 1999; Pérez-Pinzón, 2004). The statistics of stroke and cardiac arrest in this country necessitate the need for a clinically useful therapeutic intervention. However to date, most clinical trials have failed. While the value of IPC in conferring neuroprotection is very difficult to implement clinically, it is important to study because it shows that it is possible for neurons to not succumb to cell death following a lethal bout of ischemia. Also, it is widely believed that understanding how IPC works mechanistically will eventually lead to therapies for both stroke and cardiac arrest brain damage that will be effective in the clinical setting.

1.5.2 Immediate versus Delayed Preconditioning

Classically, the preconditioning paradigms are categorized as either immediate (rapid) or delayed preconditioning. This designation is based on the time which is

allowed to elapse between the introduction of the sublethal insult (i.e. the preconditioning event) and the subsequent lethal ischemic insult. In an immediate preconditioning paradigm, the sublethal preconditioning insult is given very shortly (1-30 min) before the subsequent lethal ischemic insult occurs (Barone et al., 1998). Whereas delayed preconditioning is based on an extended timeline in which the lethal ischemic insult is administered 24-48 hr after the initial preconditioning insult (Puisieux et al., 2004).

Immediate preconditioning has been widely investigated and applied to myocardial tissue with promising results, whereas its utility has been more questionable in cerebral ischemia, with mixed reports of its success in conferring neuroprotection (Stetler et al., 2009). In 1997, Pérez-Pinzón and colleagues first reported the effects of immediate IPC on vulnerable rat CA1 neurons. In this study they employed the 2VO/HT model to induce global brain ischemia. In line with the immediate IPC paradigm, they administered a sublethal ischemic event for 2 min, followed by 30 min of reperfusion, after which they initiated the 10 min ischemic insult (Pérez-Pinzón et al., 1997). They observed that in comparison to control animals that only underwent 10 min ischemia, there was reduced histopathological cell death in the IPC group when examined after 3 days reperfusion. However, hippocampal cell death after 7 days reperfusion was not significantly different between the preconditioned and non-preconditioned groups (Pérez-Pinzón et al., 1997). These results suggested at the time that the immediate preconditioning paradigm in the brain was a transient phenomenon.

Conversely, much work has also been done to investigate the potential role of delayed preconditioning on conferring neuroprotection. In the early 1990s, multiple investigators preceding Pérez-Pinzón and colleagues studied the delayed

preconditioning paradigm in the context of global brain ischemia. In these earlier studies both groups (Kato et al., 1991; Kitagawa et al., 1991) used bilateral carotid artery occlusion to achieve global ischemia and their preconditioning event consisted of 2 min of ischemia followed by 2 days reperfusion prior to the lethal ischemic insult. They observed that the neuroprotection conferred during this delayed preconditioning protocol was significant, preventing neuron death up to 7 days after the long duration ischemic insult. The significant preservation of the hippocampal CA1 neurons in this study demonstrated that delayed preconditioning was very protective of CA1 neurons. Compared to the maximum protection of 3 days observed after immediate IPC, these results were important in demonstrating the robust and long term effect of protection produced when the preconditioning stimulus was allowed sufficient time to set in before the lethal insult.

Years later in a 2004 study, Pérez-Pinzón et. al (2004), compared the two different windows of neuroprotection afforded by either immediate or delayed preconditioning. They replicated their results from their earlier study on immediate IPC, that rapid IPC could only protect against histopathological changes for up to 3 days of reperfusion but not 7 days (Pérez-Pinzón et al., 1997), and in addition they also performed delayed preconditioning to measure its protective capacity (Pérez-Pinzón, 2004). For delayed preconditioning, they followed the exact same procedure as above except the reperfusion period between the IPC and prolonged ischemia was 48 hr, as opposed to 30 min. This set of data revealed that following delayed preconditioning, there was a robust and long-lasting neuroprotection, as demonstrated by 33% protection of normal neurons by the 7th day of reperfusion (Pérez-Pinzón, 2004). Again, this asserted the idea demonstrated years earlier, that delayed preconditioning offers a

more long-term protection against cell death in vulnerable neurons.

Despite the results from the 1997 study showing that immediate IPC could confer short-term, transient neuroprotection, the majority of the field as well as the literature has continued to focus more heavily on the concept of delayed preconditioning in brain ischemia. The fact that the neuroprotection conferred during delayed IPC has proven to be more robust, and long-lived than that of immediate IPC has made it a more worthwhile avenue to pursue. However, the disparity in the protection of vulnerable hippocampal neurons as revealed in these studies of immediate versus delayed IPC, seems to suggest that some variation exists in the underlying mechanism(s) of preconditioning as it occurs over different time courses. This has introduced another set of issues to be resolved, before IPC can truly be of utility in any setting. The fact that two distinct time frames of IPC can produce drastically different results in overall protection from cell death makes the investigation into the underlying mechanisms of neuroprotection all the more relevant.

1.5.3 Gene Expression and Ischemic Preconditioning

The molecular mechanisms of IPC responsible for conferring neuroprotection are still incompletely understood. Yet, studies like the ones reviewed above discovered that ischemic tolerance requires at least 24 hours to manifest, achieves maximal intensity at 3 days, and persists for about a week (Puisieux et al., 2004; Simon et al., 2007). This time course has highlighted the roles of protein synthesis and altered gene expression in IPC induced tolerance. There are two schools of thought in regards to alteration of gene expression during IPC: 1.) preconditioning results in gene suppression to confer a protected phenotype, or 2.) IPC leads to the induction of *de novo* protein synthesis to upregulate levels of protective proteins. I will return to a discussion of the latter;

however, it is important to address both in the context of ischemia to develop a complete picture.

Roger Simon's group has done a significant amount of work investigating the role of gene suppression, and they propose that the basis of developing tolerance lies in the ability of preconditioning to genetically reprogram the cell's response to ischemia (Stenzel-Poore et al., 2004; Simon et al., 2007). In their model of focal ischemia via middle cerebral artery occlusion (MCAO), they employed a delayed preconditioning paradigm consisting of 15 min occlusion, 72 hr reperfusion (preconditioning event), followed by 60 min of occlusion, essentially to replicate preconditioning plus stroke. Using microarray analysis, they found that following IPC plus stroke, there was widespread down regulation in a number of genes, but primarily those involved in metabolism and the processes of synaptic transmission/transport (Stenzel-Poore et al., 2004). Interestingly, these genes were shown not to be down regulated during conditions of stroke alone. These results suggest that the reprogramming role of preconditioning is to dampen overall cellular activity resulting in decreased expenditure of cellular energy and preservation of cellular homeostasis. They liken this profile to one of hibernation and continue to support the notion that changes in gene expression during preconditioning must essentially incorporate overall gene suppression of high-energy utilizers in order to achieve a protected state.

Other investigators have taken a different approach from Simon's group and have undertaken studies to systematically evaluate the role of preconditioning induced ischemic tolerance. The observation that it requires at least 24 hours to induce ischemic tolerance, reasonably suggests that this process directly involves the synthesis of neuroprotective proteins. There has been much disagreement to date

regarding the exact identity of genes thought to be up-regulated during preconditioning, and thus remains a highly investigated area. Among the proteins focused on in IPC, the heat shock proteins (HSPs) remain popular subjects of study. HSPs are highly conserved molecular chaperones, which facilitate protein folding (Stetler et al., 2009). During the induction of stress, they improve cell survival by buffering the rapid accumulation of protein aggregates and denatured proteins (Stetler et al., 2009).

In an early study by Kirino et. al (1991), they subjected gerbils to preconditioning of 2 min ischemia plus 2 or 4 days reperfusion and then a subsequent ischemic insult of 5 min. Using immunocytochemistry with an anti-body against HSP70, their data revealed a definite increase in HSP70 protein staining within the hippocampal CA1 neurons following 2 min ischemia, 2 day reperfusion (Kirino et al., 1991). Even after 4 days reperfusion following the 2 min ischemia, staining was still as intense as in the 2 day reperfusion group, whereas the HSP70 immunostaining was faintly detectable in the CA1 pyramidal neurons of animals not subjected to the preconditioning event prior to the 5 min ischemia. This initial study was significant in demonstrating the upregulation of HSP70 during the 2 day window of preconditioning, thus indicating its possible role in conferring tolerance.

Later on another group Zhao et. al (Zhao et al., 2006), used the MCAO model of focal ischemia to also evaluate the role of protein synthesis in preconditioning induced ischemic tolerance. They evaluated infarct size, neurological deficits, and HSP70 expression both with and without preconditioning in order to determine its effects in building tolerance. They also employed the use of cycloheximide (CHX), as described above, a well-known protein synthesis inhibitor, to evaluate the role of total protein synthesis in preconditioning. They observed that when CHX was given just prior to the

preconditioning (sublethal) ischemia, it inhibited all subsequent protein synthesis for the duration of 24 hr, and consequently the CHX pre-treated, preconditioned group showed no reduction in infarct size as compared to their vehicle treated preconditioned counterparts (Zhao et al., 2006). In the second part of the study, they administered the same dose of CHX 30 min before the 2nd (lethal) permanent MCAO (i.e. after the 24 hour window following preconditioning), and they observed a reduction in percent infarct size in both the vehicle and CHX treated groups compared to the controls. These results taken together emphasize the significance that blocking protein synthesis has on the ability of the preconditioning event to develop ischemic tolerance. When protein synthesis is completely inhibited in that critical window 24 hours following the sublethal preconditioning event, the end result is that the cells are no longer protected in the same manner or to the same degree as when protein synthesis is permitted during preconditioning. Taking it one step further, they also assessed the levels of HSP70 protein via Western blot analysis in the 24 hour period after the preconditioning event was initiated. They observed an increase in HSP70 protein during this period compared to the sham-operated controls. However, when CHX was administered prior to preconditioning, the expression of HSP70 in the CHX treated preconditioned group was significantly decreased compared to vehicle-treated preconditioned counterparts. Furthermore, protein synthesis in the CHX pretreated group no longer significantly differed from the expression of that in the sham-operated control group.

Overall these results demonstrate that the preconditioning paradigm is a powerful inducer of ischemic tolerance and moreover, the tolerance that is established in this critical window of preconditioning is dependent on the *de novo* synthesis of proteins. When protein synthesis is compromised or inhibited, so too is the protective mechanism

that preconditioning is based upon.

1.6 Summary and Proposed Hypothesis

Thus far, I have introduced the overall problem of how TA occurs during periods of reperfusion following global brain ischemia. I then presented information correlating prolonged translation arrest with DND of the vulnerable hippocampal CA1 pyramidal neurons following brain I/R. I discussed how the alteration in translation initiation factors, primarily the phosphorylation of eIF2α, initially inhibits translation in the post-ischemic brain, but is not a sustained event and cannot explain prolonged TA. Finally, I reviewed recent work from our laboratory that identified the sequestration of translational machinery into novel ribonomic structures, termed mRNA granules, as the event leading to the persistent TA in neurons that eventually succumb to DND. This same body of work also presented information that demonstrated that the HuR colocalization within mRNA granules was directly correlated to translation of HSP70 protein. I then briefly reviewed IPC, a highly effective paradigm for neuroprotection, and discussed how its role in conferring neuroprotection is dependent upon protein synthesis.

That IPC depends on protein synthesis and is abolished in the presence of CHX is significant for our lab's results with CHX and mRNA granules. As reviewed above, ischemia itself causes TA. Thus, the action of CHX cannot be to simply inhibit translation, because it is already inhibited by I/R. However, our lab showed CHX to inhibit mRNA granule formation. This suggests that CHX may abolish IPC by inhibiting mRNA granules, which in turn suggests that IPC may be mediated by the RNA operon action of mRNA granules in carrying out the stress reprogramming of ischemic neurons. These considerations lead to the main hypothesis for this thesis. I hypothesize that:

mRNA granules are a protective phenomenon that allows stress reprogramming of post-ischemic neurons.

I will test this hypothesis by studying HuR colocalization with mRNA granules in CA1 neurons following IPC. I predict that, after an IPC stimulus, CA1 neurons will behave like CA3 neurons following a CA1-lethal 10 min insult and show colocalization of HuR with mRNA granules. A corollary of this hypothesis will be to investigate the effect of varying duration of ischemia on mRNA granule formation, because it is not known if 2 min of ischemia, the standard IPC stimulus, even induces mRNA granules.

I will carry out the following experiments to test these hypotheses:

[1] *Experiment 1: Using poly-A FISH, assess mRNA granules at 2,4,6,8 min ischemia.*

[2] *Experiment 2: Assess HuR and mRNA granules colocalization after 2 min ischemia plus 2 days reperfusion (IPC), and then 10 min ischemia and 1 hr of reperfusion.*

[3] *Experiment 3*

    a. *3A: Assess the effect of Cycloheximide on HuR and mRNA granules colocalization after IPC, and then 10 min ischemia and 1 hr of reperfusion.*

    b. *3B: Assess the effect of CHX + IPC on cell survival at 7 days reperfusion following 10 min ischemia.*

CHAPTER 2

Effect of Ischemic Duration on the Formation of mRNA Granules

2.1 Hypothesis Stated

I previously discussed how mRNA granules may play a role in IPC-induced tolerance against neuronal death caused by ischemia. A prerequisite to studying this phenomenon is to determine the dependence of mRNA granule formation on ischemia duration. To date, this has never been investigated in any study and thus provides a basis for the work presented in this chapter. The hypothesis of the studies described in this chapter is:

The formation of mRNA granules during reperfusion is a function of the duration of the preceding ischemia.

2.2 Experimental Overview

The 2VO/HT model was employed to induce global brain I/R in male Long Evans rats. The experimental groups (n = 3 per group) consisted of rats exposed to 2 min (2I), 4 min (4I), 6 min (6I), and 8 min (8I) of ischemia, each followed by 1 hour of reperfusion. The control group was sham-operated non-ischemic controls (NIC). At 1 hr reperfusion, experimental animals were anesthetized, and, along with NICs, perfusion fixed, and 50 micron tissue slices through the dorsal hippocampus were prepared. Slices were stained by double-labeling immunofluorescence histochemistry (IF)/FISH for HuR and poly-A to assess formation of mRNA granules and HuR-poly-A colocalization. To quantify the extent of colocalization of HuR and poly-A mRNA granules in CA1, five additional 4I animals were performed and compared to rats subjected to 10 min ischemia and 1 hr reperfusion (10I, n = 5).

2.3 Experimental Procedures

2.3.1 Materials

The two Alexa Fluors used for IF histochemistry, Alexa FluorR 488 donkey anti-goat IgG and Alexa FluorR 555 anti-mouse IgG, were purchased from Molecular Probes (Eugene, OR). The normal donkey serum was purchased from Sigma-Aldrich (St. Louis, MO). The 5'-biotinylated 50-mer oligo-dT probe was ordered from Integrated DNA Technologies, Inc (Coralville, IA). Prehybridization and hybridization buffers were purchased from Ambion (Austin, TX). Alexa 488-labeled strepavidin (S32354) was purchased from Invitrogen (Eugene, OR) and the biotinylated goat anti- strepavidin (BA-0500) was obtained from Vector Laboratories (Burlingame, CA). HuR (sc-5261) antibody was purchased from Santa Cruz Biotechnology (Santa Cruz, CA). All other chemicals were reagent grade.

2.3.2 Animal Model

All of the following animal experiments were approved by the Wayne State University Animal Investigation Committee and were performed in accordance with the *Guide for the Care and Use of Laboratory Animals* (National Research Council, revised 1996). In order to induce a state of global brain ischemia in our rat model, the bilateral carotid artery (two-vessel) occlusion and hypovolemic hypotension (2VO/HT) model was performed (Smith et al., 1984).

At the onset of surgery, anesthesia was induced with a loading dose of 5% halothane. Thereafter, a sufficient maintenance dose of 2% halothane in 100% O_2 was administered throughout the duration of the surgery using a nosecone. Core body temperature was closely monitored with the use of a rectal temperature probe. During the ischemic period and 1 hr reperfusion period, core body temperature was kept

constant at 37 ± 0.5° C with a homeostatic blanket system. Temporalis muscle temperature was monitored with a thermistor and head temperature was maintained at 37 ± 1° C by a heat lamp. Three major incisions were made. The tail artery was first accessed and exposed for the placement of a small catheter. This served as the port to monitor mean arterial pressure (MAP) in real-time during the entire procedure. Next, a vertical ventral incision was made at the neck in order to gain access to the common carotids for induction of ischemia. Here, the external carotid arteries were carefully isolated bilaterally, being careful to avoid perturbing the vagus nerve. A third incision was made near the hind leg in order to access and catheterize the femoral artery for blood withdrawal to achieve hypovolemia. Upon completing surgery steps, ischemia was induced by first removing 10 cc of blood until MAP was 50 mmHg. The bilateral carotid arteries were then immediately clipped using micro-aneurysm clips, and the appropriate amount of time was allowed to pass (2, 4, 6, or 8 min) to achieve the desired period of ischemia. The clips were then removed and blood was reinfused back into circulation via the femoral port. Animals were maintained under anesthesia with temperature control for the 1 hr reperfusion period. At 1 hr reperfusion, animals were sacrificed by transcardial perfusion fixation.

2.3.3 Perfusion Fixation/Tissue Slicing

Solutions for the fixation process, 0.9% NaCl and 4% paraformaldehyde (PFA) in 0.1 M phosphate buffered saline (PBS), were prepared in advance and stored at 4° C prior to use. Rats were perfused transcardially first with 250 ml of ice cold 0.9% NaCl, followed by 300-350 ml of 4% PFA at a rate of 47 ml/min and 30 ml/min, respectively. Following perfusion, brains were carefully dissected so as to not damage the tissue, and stored in vials containing 4% PFA for the post-fixation period ranging from 24-48 hrs.

Post-fixed brains were sliced in the coronal plane using a vibratome to obtain 50 μm thick slices. The tissue was sectioned accordingly in 0.1 M PBS solution and each slice was placed in individual wells of a tissue culture dish filled with cryoprotectant solution. All tissue was stored at -20° C in cryoprotectant solution until stained.

2.3.4 Immunofluorescence (IF) and Fluorescence *In Situ* Hybridization (FISH)

All concentrations of primary and secondary antibodies used in the immunolabeling protocol were previously determined by testing a series of dilutions on control and experimental samples (Jamison et al., 2008).   Double IF/FISH immunolabeling was performed in two stages over a 3 day period.

Immunofluorescence (IF) was carried out over the first 2 days. Prior to staining, sample brain slices were washed in 0.1 M PBS solution for 10 min X4. Following the washes, the samples underwent a preblock step in a solution containing 0.3% Triton X-100 dissolved in 0.1 M PBS (PBS-Tx) and mixed with 10% normal donkey serum (NDS), the same species as the secondary antibody. Slices were gently rocked in 330 μl of preblock solution for 25 min. Next, samples were washed for 10 min X3 in PBS and then 330 μl of primary HuR antibody (1:25 concentration) diluted in 1% NDS and PBS-Tx was applied and allowed to incubate on a rocker at room temperature overnight. The primary antibody was then removed the following day and samples were again rinsed for 10 min X3 in PBS solution. Following the final wash step, secondary antibody (1:300 concentration) was prepared under low light illumination in 0.1 M PBS-0.3% Tx-10% NDS and 330 μl was applied to each sample and left to rock for a 2 hr incubation period. Slices were then mounted onto lysine-coated slides in a 0.1 M PBS solution. After mounting, slices were fixed for 10 min in 330 μl of 3.6% formaldehyde in distilled water, and fixative was drained from slides by blotting on a paper towel.

The second stage, FISH, was performed immediately following fixation of the IF stage using a modified procedure of (Bessert and Skoff, 1999). The entire FISH protocol was performed under low light illumination or in the dark. The first step was a 3 hr prehybridization period performed in an incubator at 32° C in which prehybridization buffer was placed on each slide and then placed within a box humidified with 50% formamide/4X saline-sodium citrate (SSC). Using the same apparatus, slides were incubated overnight at 32° C in a solution containing 50 ng/ml 5'-biotinylated 50-mer oligo-dT probe dissolved in the same hybridization buffer from the previous step. All subsequent processing of tissue was performed in the dark at room temperature the following day. Slides were washed in 2X SSC for 10 min X3 and then incubated for 60 min in a solution containing 1:500 Alexa 488-labeled strepavidin in 4X SSC 0.1% TritonX-100. The solution was removed and slides were washed for 10 min in 4X SSC after which, a solution of 1:667 biotinylated goat anti-strepavidin dissolved in 2X SSC/0.1% Triton X-100 was applied and allowed to incubate for 60 min. Slides were washed once more in 4X SSC for 10 min and then the final incubation was performed for 60 min in a solution of 1:667 Alexa 488-labeled strepavidin in 2X SSC/0.1% Triton X-100. Following the final incubation and prior to coverslipping, the slides were sequentially washed in 4X SSC and 2X SSC for 10 min each. Slides were coverslipped using Vectashield hard-set and stored at -20° C until they could be imaged. The specificity of the poly(T) probe for poly-A mRNA was previously validated as described by (Jamison et al., 2008) where it was shown that poly-A signal was abolished following prior incubation of slices in RNAse or 0.1 M NaOH, but not DNAse.

2.3.5 Microscopic Analysis and Data Acquisition

Data Acquisition

Evaluation of all slides was performed using photomicrographs obtained from an ApoTome-equipped Axioplan 2 Imaging System (Carl Zeiss, Oberkochen, Germany) under 63X oil immersion magnification. Excitation and emission for Alexa 488 (green) was 488 nm and 518 nm, respectively. Excitation and emission for Alexa 555 (red) was 568 nm and 600 nm, respectively. The ApoTome-equipped system uses a grid in the aperture plane to optically section samples. This feature is designed to reduce extraneous light scattered from other focal planes and thus produces images with exceptional sharpness.

The term "optical sectioning" refers to the individual images obtained at discreet focal planes throughout the depth of a sample. For each focal plane, the computer program, working in conjunction with the ApoTome, acquires images of the specimen's multiple layers and separates them by a defined distance. The recorded set of photomicrographs consisting of sequential optical sections is known as a z-stack. We collected stacks of z = 10 optical sections, separated by distances of 0.35 microns. All images were collected at 1388 x 1040 pixel resolution, corresponding to x and y distances of 0.102 microns per pixel edge. For each brain slice, photomicrographs of CA1 and CA3 were obtained bilaterally at the level of the dorsal hippocampus, resulting in four z-stacks per animal.

Data Analysis

A. Orthographic Projections. For each z-stack, a maximum intensity orthographic projection was constructed in NIH ImageJ (Abramoff et al., 2004). An orthographic projection "blends" all z-slices to produce a single image. The term "maximum intensity"

projection means that the corresponding pixels from each slice are added together. The final image is then normalized to the mean brightness of the input images. While a single z-slice has excellent focus, the light intensity has been reduced > 95% from the original image. Therefore, orthographic projections are constructed to amplify the signal and make subcellular structures, such as mRNA granules, more distinct for subsequent analyses. Additionally, since the projections reduce the 10 images per stack to a single image, this helps simplify downstream analyses.

B. mRNA granules as a function of ischemia duration. Next, all orthographic projections were input into Adobe Photoshop and compiled into a single large composite image so all samples could be viewed side by side. Using these composite images for CA1 and CA3, the number of samples containing mRNA granules was counted per region per experimental group, and then expressed as the percentage:

$$\frac{\text{number of samples containing mRNA granules per group per region}}{\text{total number of samples per group per region}} x100\%$$

Graphs of percentages were plotted against the duration of the ischemia and either fit by linear regression or by a Hill function using the function fitting routine in Matlab (ver. R2012a). The Hill equation outputs a value ranging from 0 to 1 and corresponds to the function, $f(x) = \frac{x^n}{x^n + b^n}$ where: x = the time of ischemia in min, n = the Hill coefficient and b = the threshold duration of ischemia at which 50% of rats have mRNA granules in their neurons. At low values of n, the function approximates a linear relationship. By plugging increasing values of n into the above equation, the function will gradually resemble the classic sigmoidal curve (DeGracia et al., 2012). When n is large ($\sim$ > 20), the function assumes a square wave at the threshold value b. This demonstrates an on/off effect at the threshold. We allowed Matlab to find the optimal

values of both *n* and *b* for the Hill equation fits.

  C. Colocalization of HuR and poly-A. In a double-labeling experiment where two distinct antibodies are represented in separate channels, such as red and green, a specific type of analysis must be employed in order to determine the overlap or extent to which the channels co-vary. This colocalization analysis incorporates mathematical techniques to determine the extent to which the two staining patterns differ. These standard techniques involve evaluating all pixels contained within an image, however, in the current study this proved to be too broad of an application since our aim is to investigate the colocalization of HuR with mRNA granules in neuronal cytoplasm. Therefore, the adapted method used in the current analysis is described below. A sample image from the analysis is shown in Figure 6, and is followed by a summary of the steps performed in the analyses.

  The procedure for generating the image in Figure 6 consisted of 5 steps. They are

Merge → Yellow Channels → Mask Nuclei → Yellow Cytoplasm → Remove Background
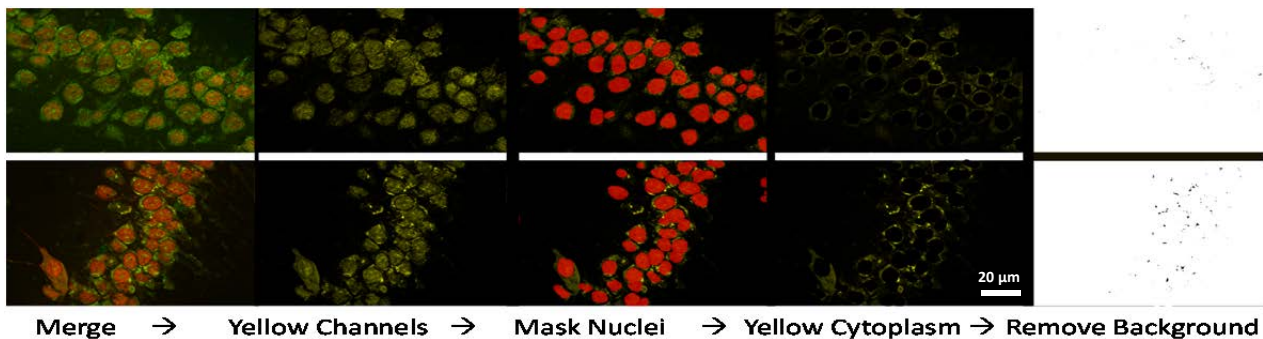
Figure 6. Images showing how colocalization is measured. Fluorescent images show the procedure for measuring colocalization of HuR and poly-A in the cytoplasm of hippocampal CA1 neurons. The top panel corresponds to a sample from a non-ischemic control (NIC). The lower panel shows neurons from an animal exposed to 4I, 1hR. From left to right, the panels are (1) Regular merged images, (2) yellow channels falsely colored yellow, (3) yellow channels with the nuclei masked, showing the masks, (4) yellow channels with the masks subtracted, (5) yellow channels shown as inverted gray scale images. The inverted gray scale images were counted for optical density (OD) in the program ImageJ. Scale bar = 20 μm; applies to all panels.

as follows: (1) calculate the yellow channel, (2) mask all nuclei in the yellow channel to effectively eliminate their contribution to the signal, (3) eliminate residual background signal, (4) perform densitometric analysis on the resulting images, (5) average the densities for experimental groups and test for statistical significance.

Step 1: *Calculate the yellow channels.* The first step is to generate a "yellow channel" (Kayali et al., 2005). When an image is merged in a double-labeling study containing green and red fluorophores, a graded yellow color is observed anywhere a given pixel has signal in both channels. Since each channel is an 8 bit image, this means that a maximum of 256 (2^8) colors or shades of gray (when viewed in gray scale), can be displayed at any one time. This means that each intensity of gray within the gray scale image corresponds to a certain numerical value ranging from 0-255, where no signal is represented by 0, and maximum signal (or light intensity) is represented by 255. Essentially, what this process does is define the light intensity of each individual pixel within an image as a numerical value. Taken together, each digital image can be thought of as a 2x2 matrix of numbers. The number of columns of the matrix equals the *x* resolution in pixels, and the number of rows represents the *y* resolution in pixels. Since each channel varies with respect to light intensities and thus represents its own separate matrix, a standard merged image can be obtained by performing a mathematical operation on the two input matrices (i.e. the red and green channel for each image).

When the two input matrices are displayed as a merged image, the operation is known as the set operator **union**, where red, green, and their overlap is displayed. However, it is also possible to perform other set operations on the channels. For example, one can calculate the **intersection** of the two input channels. The resulting

intersection displays only the pixels where the two channels overlap, ultimately eliminating the presence of the separate red and green signals. The "yellow channel" is exactly this operation of intersection applied to the two input channels. Therefore, our first step is to take each orthographic projection and calculate the intersection of the two channels. This is performed in Adobe Photoshop by applying the "multiply" calculation to the red and green channels. Any overlap between red and green pixels results in the production of a new channel, which we call the yellow channel.

Step 2: *Masking of images.* Since we are only interested in the overlap of signal in the neuronal cytoplasm, we used Photoshop to manually mask the nuclei of all input images. This step is important because substantial HuR and poly-A overlap appears in the nucleus. However, this has no bearing on the current analyses because the nuclear colocalization has been shown not to change as a function of brain I/R (Jamison et al., 2008; Szymanski et al., 2012). Yet, since the nuclei occupy a large cellular area, the corresponding amount of colocalized nuclear signal is also very large. Thus, it would eliminate any differences between groups if left in the densitometric analysis. Therefore, by masking the nuclei, this nuclear signal is removed from the images. This step is feasible because HuR staining results in visualization of clearly defined nuclei (Szymanski et al., 2012) which are then easy to see and manually mask.

Step 3: *Resetting yellow channel baselines to eliminate background signal.* Similar to nuclear colocalization, there is also a low level of HuR/poly-A colocalization in the cytoplasm. This baseline amount of colocalization does not represent mRNA granules since it is present in NIC samples known to lack mRNA granules (Jamison et al., 2008; Szymanski et al., 2012). This constitutes a background signal within which true mRNA granules are embedded and thus needs to be accounted for. By resetting

the baseline of the yellow channels, it effectively sets the background signal to zero. In order to subtract this background colocalization signal, it is first necessary to measure the density of nuclear-masked yellow channels in NIC samples. With the nuclei masked, this gives a measurement of the yellow channel density present in only the cytoplasm. The density from several NIC samples is measured and then averaged. This average now accounts for the residual yellow background. Finally, this average yellow density can be subtracted from the average yellow density of all experimental group samples to yield whatever yellow density remains in the cytoplasm. When this average background density is subtracted from NIC samples, it sets the density of those samples to zero. Yet, when that average background density is subtracted from the average density of reperfused samples containing any significant amount of additional yellow signal in the cytoplasm, it will yield a signal greater than the NIC average.

Step 4: *Measuring density.* To measure density of the nuclear-masked yellow channels, they are taken into NIH Image J which has the capacity to measure the pixel density (optical density, OD) of any 8 bit region of interest (ROI). The entire nuclear-masked yellow channel is measured for each control and experimental sample, and then tabulated in Microsoft Excel. The NIC group is first averaged, and this average, as explained above, is subtracted from each individual sample of the experimental groups, and each experimental group is then averaged. The resulting data is then tested for statistical significance using Student's t-test for 2 group comparisons or ANOVA for comparing more than 2 experimental groups. The p values are calculated in Excel and reported with the data. In line with the universally accepted rule for statistical significance, groups were considered to be different if $p < 0.05$.

2.4 Results

2.4.1 Formation of mRNA Granules with Varying Ischemia Duration

We observed that mRNA granules formed in all ischemia duration groups. Representative samples are shown in Figure 7. The frequencies of rats in each group containing mRNA granules are tabulated in Table 1. It is known that NIC rats contain zero mRNA granules in their neurons (0% frequency), and 100% of rats subjected to 10 min ischemia, will possess mRNA granules in CA1 and CA3 neurons at 1 hr reperfusion (Jamison et al., 2008). We can use these as end-points in plots that show the frequency of mRNA granule-containing rats vs. ischemia duration for CA1 and CA3 (Figure 8). The curves in Figure 8 appear very similar and approach 100% by 6-8 min ischemia.
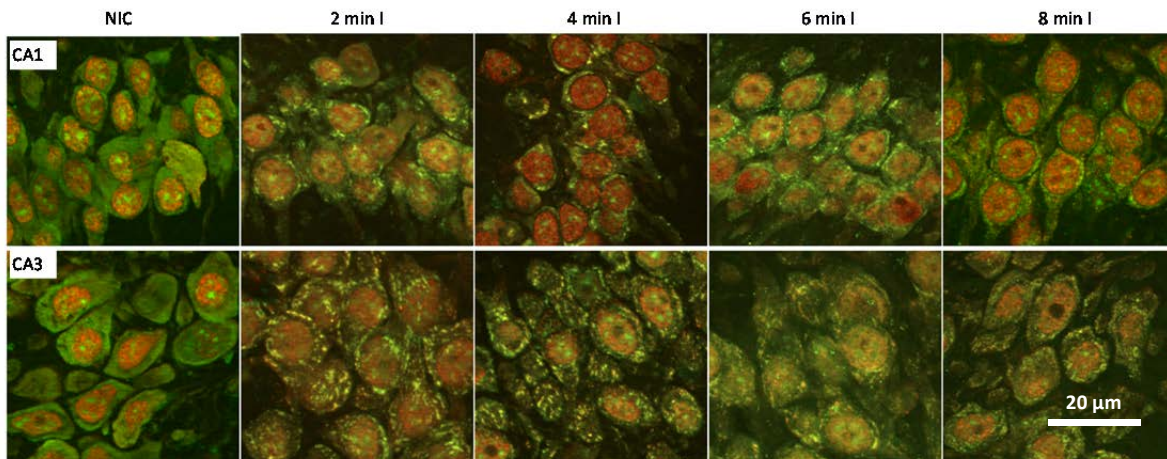
Figure 7. mRNA granules at varying durations of ischemia. The above images are examples showing mRNA granules at the tested durations of ischemia: 2, 4, 6, and 8 min I, followed by 1 hr reperfusion. Upper panel is taken from CA1 neurons and the lower panel shows CA3 neurons. Staining was poly-A FISH (green) and HuR (red). mRNA granules are visible in all ischemia groups. Scale bar = 20 μm applies to each.

Table 1. Frequencies of rats with mRNA granules for durations of ischemia and hippocampal regions CA1 and CA3.

	2minI	4minI	6minI	8minI
n, total	3	8	3	3
# yes CA1	2	6	3	3
% yes CA1	67%	75%	100%	100%
# yes CA3	2	7	2	3
% yes CA3	67%	88%	67%	100%

Two types of regressions were conducted on this data. Linear regressions are plotted in Figure 8, along with the fit equations and the correlation coefficients (R^2). The slope and y-intercepts were almost identical for CA1 and CA3, and the R^2 values were 0.73 and 0.68 for CA1 and CA3, respectively. The relatively low R^2 values indicate that fitting to a straight line was not ideal. Since the data plotted in Figure 8 more closely resembled an S-shaped curve, we also fit it to the Hill equation.
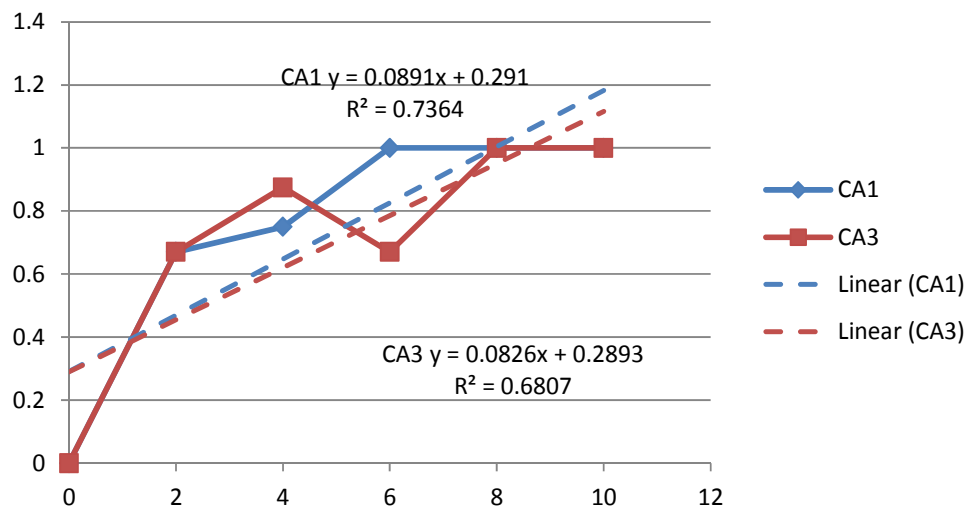
Figure 8. The appearance of mRNA granules as a function of ischemic duration. The plot shows the proportion of rats in each group that displayed mRNA granules. The proportion of rats with mRNA granules approaches 100% by 6-8 min of ischemia in both CA1 and CA3.

Figure 9 shows the data points fit to the Hill equation. The parameter *b* represents the threshold duration of ischemia at which 50% of rats have mRNA

granules in their neurons and *n* is the Hill coefficient. The values from the Hill fits were:

CA1: $b = 1.43 \pm 0.55$ and $n = 1.78 \pm 0.88$

CA3: $b = 1.10 \pm 1.15$ and $n = 1.16 \pm 1.00$

Problematically, the lower bound for the standard deviations (-2σ) for *b* and *n* for the CA3 fit gave negative values of -1.205 and -0.857. A negative value for *b*, the threshold duration of ischemia whereby 50% of rats show mRNA granules, physically does not make sense. In addition, the Matlab curve fitting routine identified the CA3 6I
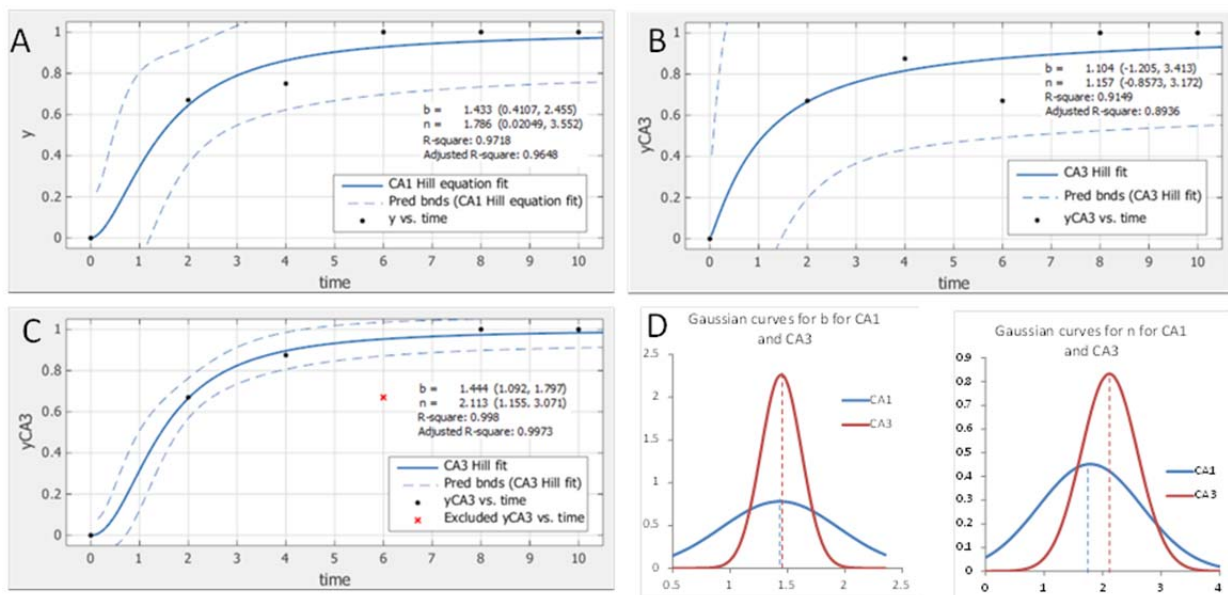
Figure 9. Hill Equation Fits. Since the data points closely resembled an S-shaped curve, they were fit to the Hill equation accordingly, **(A)** CA1, **(B)** CA3, **(C)** CA3 with outlier removed. **(D)** Gaussian distributions of the threshold, *b*, and Hill coefficient, *n* for CA1 (blue curves) and CA3 (red curves).

group frequency point as an outlier. Simply looking at the points plotted in Figure 8, this made sense because if 4I led to 88% of rats showing mRNA granules, then 6I must be equal to or greater than the 4I value, but it is less in our data (Table 1). Thus, the Hill equation fit was re-run treating the 6I CA3 point as an outlier (Figure 9C), resulting in new values for the CA3 fit of $b = 1.444 \pm 0.17$ and $n = 2.113 \pm 0.48$. For the Hill fits, the adjusted R^2 values for CA1 and re-fit CA3 were 0.97 and 0.99, respectively,

considerably better than the linear regression.

Figure 9D shows the Gaussian distributions of *b* and *n* for CA1 and re-fit CA3. Although the CA1 curve is broader, it lies directly on top of the CA3 curve for the *b* parameter. In terms of the *n* parameter, the values do not clear statistically between CA1 and CA3, but the two Gaussian curves are not identical and the mean value of *n* for CA1 is less than that of CA3. Results from the Gaussian curves for parameter *b* indicate that the threshold duration of ischemia for forming mRNA granules is the same between CA1 and CA3, approximately 1.4 min of ischemia. This indicates that the formation of mRNA granules in neurons is extremely sensitive to the duration of ischemia. Additionally, the result for the *n* parameter Gaussian distribution suggests, but clearly does not prove, that the difference in response between CA1 and CA3 lies in factors that could be represented by the Hill coefficient. In terms of its meaning, *n* is traditionally a measure of "cooperativity" or how the parts of the system interact to carry out the process being modeled by the Hill equation. These points will be elaborated in the discussion of this data in Chapter 5.

2.4.2 Colocalization of HuR and mRNA Granules after 4 min and 10 min Ischemia

It was previously observed that HuR colocalized with mRNA granules in resistant CA3 neurons at 1 hr reperfusion after 10 min ischemia, but did not colocalize in vulnerable CA1 (Jamison et al., 2008). Therefore, it was of special significance to observe that some of the lesser durations of ischemia, as shown in Figure 7, showed colocalization of HuR and mRNA granules in the cytoplasm of CA1 neurons. Because the study of varying ischemic durations showed this colocalization to be the greatest in the 4I group, we added five additional animals to this experimental group. We then applied the procedure described above (Figure 6) to quantify cytoplasmic HuR and poly-

A colocalization in CA1 of the 4I group versus legacy samples of the 10 min ischemia, 1 hr reperfusion group (10I).

Figure 10 shows representative samples for the NIC, 4I and 10I groups, illustrating the (1) merged, (2) green poly-A, and (3) red HuR channels. The 4I group showed distinct granular structures in the HuR (red) channel, but the 10I group resembled NICs in the HuR channel, in spite of granular poly-A staining in both the 10I and 4I samples.
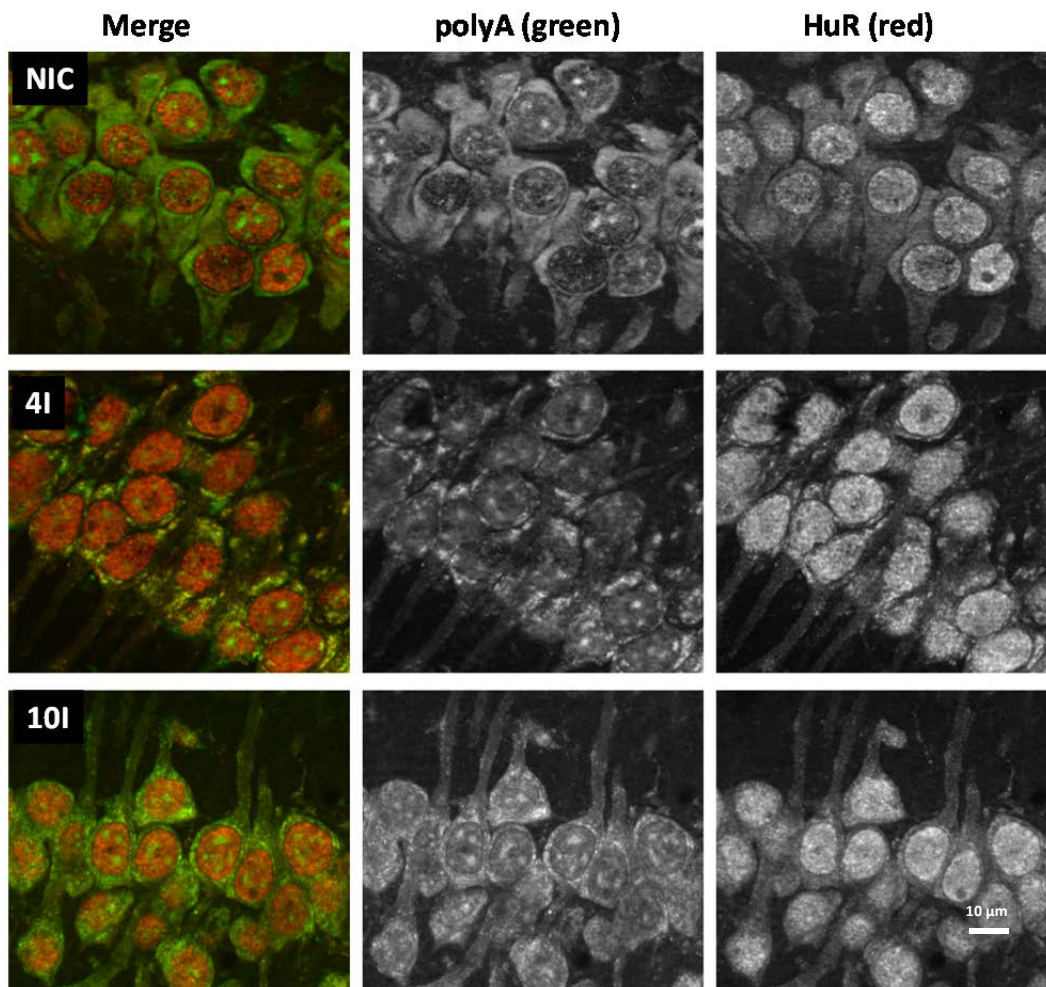
Figure 10. Contrast in HuR staining in CA1 at 4I and 10I. The colocalization of HuR with poly-A is shown in the left column as merged images for experimental groups as labeled. Individual channels for poly-A (center) and HuR (right) are also shown. Note the absence of granules in the HuR channel of 10I and NIC samples, and the corresponding lack of colocalization with poly-A in the merged image.

Figure 11A shows the respective yellow channels for the images in Figure 10, and also shows the nuclear masked yellow channels. In the 4I group there are granular structures that colocalized in both the poly-A and HuR channels, resulting in intense dark mRNA granules in the 4I yellow channel.   While the 10I yellow channel appears more granular than the NIC, the colocalized yellow signal is less intense than the 4I group.   The 3rd column shows the respective optical density of each image, and the value obtained when subtracted from the NIC value.   When 5 animals were run per group and ODs averaged, the mean density of the 4I group was about 5-fold greater than that of the 10I group, after each was normalized to the NIC group (Figure 11B), and these cleared at p = 0.041 by a Student's t-test.
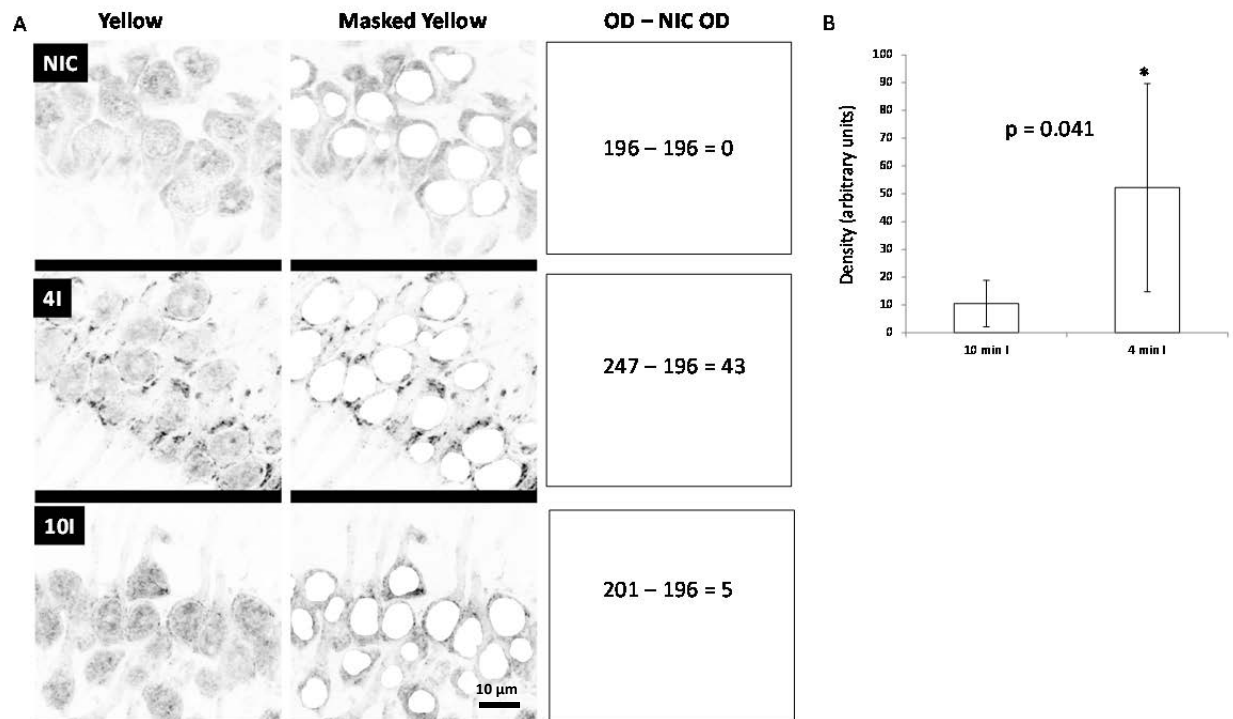
Figure 11. Yellow channels and quantification of mRNA granules. **(A)** Left: the yellow channels in gray scale corresponding to the merged image in Figure 10. Center: the yellow channels with the nuclei masked. Right: the respective optical density of each image as measured in ImageJ. **(B)** Average density (± standard deviation) of the 4I group compared to that of the 10I group. For the 4I and 10I groups, n=5. p value is result of Student's t-test. Scale bar = 10 μm; applies to all panels.

2.4.3 Summary

I showed here that mRNA granules formed at all durations of ischemia tested from 2-8 min, and there were no statistical differences in the Hill function fit of the data between CA1 and CA3; however, the parameter *n* was not identical between the groups.   Additionally, when the 4I group was compared to the 10I group for colocalization of poly-A and HuR signal in the cytoplasm of CA1 neurons, the 4I group was ~ 5X greater than the 10I and this is consistent with the qualitative observation that HuR colocalized with mRNA granules in CA1 neurons after 4 min ischemia and 1 hr reperfusion.   These results indicate that short durations of ischemia, as applied in preconditioning (e.g. 2I) have the ability to induce mRNA granule formation as well as colocalization with HuR in neurons during the reperfusion period.

CHAPTER 3

Effect of Ischemic Preconditioning on mRNA Granules

3.1 Hypothesis Stated

Since sublethal durations of ischemia induce mRNA granules, it is possible that mRNA granules contribute to IPC-induced neuronal survival following the 2nd, lethal ischemic insult. As shown in Chapter 2, at 1 hr reperfusion following 4 min ischemia, HuR colocalized with mRNA granules in CA1 neurons. This is a novel and significant observation because the colocalization of HuR and mRNA granules early in reperfusion following a lethal 10 min ischemic insult has been shown to correlate with the translation of stress proteins (e.g. HSP70) and cell survival in resistant CA3 neurons, but this colocalization does not occur in CA1 which does not translate HSP70 and does not survive (Jamison et al., 2008). However, it is unknown how neuronal mRNA granules respond after the 2nd, lethal ischemic insult, following an IPC stimulus of 2 min ischemia. Therefore, in this chapter I characterize the relationship between HuR and mRNA granule staining after rats have been subjected to 2 min ischemia and 48 hr reperfusion (IPC stimulus) followed by 10 min ischemia and 1 hr reperfusion. The specific hypothesis to be tested is:

Following an IPC stimulus, CA1 neurons will show colocalization of HuR and mRNA granules at 1 hr reperfusion after the 2nd, 10 min ischemic insult.

3.2 Experimental Overview

The experiments in this chapter compare the response following 10 min ischemia + 1 hr reperfusion, with and without IPC. The three experimental groups (n = 5/group) are: (1) NIC, (2) 10 min ischemia + 1 hr reperfusion (1hR), (3) 2 min ischemia + 48 hr reperfusion + 10 min ischemia + 1 hr reperfusion (IPC). Brain slices were prepared and

then double stained with HuR IF and poly-A FISH. The experimental groups were analyzed by **texture analysis** (Szymanski et al., 2012) to characterize the staining patterns in the three experimental groups and to correlate these to the survival or death outcome of CA1 and CA3. Texture analysis is explained in greater detail below.

3.3 Experimental Procedures

3.3.1 Materials

All materials were as described in Chapter 2.

3.3.2 Animal Model

Ischemic Preconditioning. The IPC surgery consisted of two sequential surgeries as described in Chapter 2. On day one, animals (n = 5) were subject to 2 min of normothermic global forebrain ischemia. Surgical incisions were sutured and animals returned to their cages for exactly 48 hrs reperfusion. Following the first surgery, animals were individually housed and had free access to food and water during the recovery period. At the 48 hr time point, the second surgery was performed in which animals were subjected to 10 min global ischemia followed by 1 hr reperfusion in order to evaluate the formation of mRNA granules.

3.3.3 Immunofluorescence and Fluorescence *In Situ* Histochemistry

IF and FISH techniques were performed exactly as described in Chapter 2.

3.3.4 Texture Analysis

A major difficulty encountered when trying to analyze and interpret microscope images is the fact that their analysis by visual inspection is qualitative by nature. This consequently leaves the analysis open to subjective interpretation. Qualitative analysis, by definition, rules out quantifying the changes in microscope images. As a result, this has led to the advent of multiple forms of analyses, invariably based in computer

technology, which has allowed researchers to overcome the traditional limitations in analyzing microscope data. One such method is texture analysis (TA) (Harrison et al., 2009; Szczypiński et al., 2009). TA, as the name implies, is the ability to extract information from an image based on its texture. TA derives from the computer science field of artificial vision and has its roots in mathematical methods dating back to the 1970s (Haralick et al., 1973). TA has been applied in very diverse fields in which the ability to accurately differentiate between textures in an image is critical. Examples include: characterizing radar images in meteorology (Alparone, 1990), analyzing military satellite data (Sengottuvelan, 2008), and applying robotics and machine vision (Pietikäinen, 2000). Moreover, the biological and biomedical sciences have also found increasing utility in the application of TA methods. For example, it is used for detection of non-Hodgkin lymphoma in MRI images (Harrison et al., 2009), and has been used to characterize cell behavior in microscope images of, for example, cytoskeleton rearrangement (Uppal et al., 2010), and apoptosis (Losa and Castelli, 2005).

As it pertains to the present research, the DeGracia laboratory has also adapted TA methods to quantify microscope images of poly-A staining in reperfused neurons (Szymanski et al., 2012). TA has been a valuable tool in our analyses, since mRNA granule formation after brain I/R represents a major change in the texture of the cell staining of poly-A mRNAs. However, since the main purpose of Szymanski et al. (2012) was to validate the TA methods, only CA3 was studied. I here will use the same methods, and for the first time, apply them to study the change in texture of CA1 neurons following I/R with and without IPC. A brief overview of the TA method is first given, followed by a more detailed explanation of each step.

Briefly, the steps performed in TA are as follows: (1) Obtain orthographic

projections as described above, (2) Mask the nuclei and background for each image, subtract those masks, and obtain the final cytoplasmic area, (3) Perform TA and measure 168 **texture features** of the cytoplasmic images, (4) Run feature selection using Fisher's test to reduce the 168 features to the top 10 features, (5) Perform feature projection to further reduce the 10 features to one to three principle components, and (6) Run statistics on the principle components using ANOVA to assess whether any differences exist between experimental groups.

Generating Masks

After generating the orthographic projections, as described in Chapter 2, masking of the nuclei and background is required. The purpose of masking is to ensure that only the regions of interest (ROIs) are subjected to TA while all regions of non-interest are excluded from the analysis. Since mRNA granules are cytoplasmic, the entire cytoplasmic area within each image served as the ROI.

All masks were generated in Adobe Photoshop (ver cs8) by manually "coloring in" all visible nuclei in the image. This is possible and feasible because HuR staining of neuronal nuclei is distinct and prominent so nuclei can easily be identified (see example of HuR staining in Chapter 2, Figure 10). The nuclear masks are saved as "alpha channel 1". Next, the black background is selected by the "magic wand" tool set to 25 followed by the command "select similar", and the resulting mask of the background is saved as "alpha channel 2". Alpha 1 and 2 are added to give alpha channel 3, which is then inverted, to give only the area of the image containing cell cytoplasm. Alpha channel 3 is saved as an 8 bit grayscale image and imported into the TA software, MaZda. This channel is used to generate "region of interest" files that are used as masks in MaZda.

This masking method was validated in Szymanski et al., (2012) where it was shown that masking the entire cytoplasmic area gave the average result obtained from masking individual cells, and hence was independent of the size and shape of the ROI used for TA. Once imported into MaZda, the image intensities are normalized to eliminate variation due to image histograms. Thus, by masking and measuring all the cell cytoplasms in an image as a single unit, the resulting texture features represent the normalized average of all cells in the image. Because all reperfused neurons in an image will contain mRNA granules in their cytoplasms, this step is feasible.

Texture Analysis

TA was performed in MaZda (ver 4.6). MaZda is TA software developed at Technical University of Lodz, Institute of Electronics, Sweden, in the context of the COST B11 European project for analyzing MRI data (Szczypiński et al., 2009). MaZda has the capacity to measure almost 300 texture features using 6 well-validated TA methods. Table 2, adapted from Szymanski et al. (2012), lists and briefly describes each TA method.

Table 2. Brief description of texture analysis (TA) methods calculated by MaZda.

TA method	Brief Description
histogram analysis	Computes statistical features of first-order histogram
absolute gradient method	Computes statistics of the gradient magnitude map
run-length matrix	Computes pixel runs of a given intensity along specified vectors
co-occurrence matrix	Computes statistics of change in pixel intensities a given distance and direction from a central pixel
autoregressive model	Computes intensity deviation of a central pixel from a linear weighted average of surrounding pixels
wavelet analysis	Pixel intensity changes transformed into frequencies; determines frequency components of texture

To use MaZda, the 8 bit grayscale red and green channels are imported and analyzed separately, using the mask files generated as described above. Texture features and program options are chosen and then calculated by MaZda, which outputs texture features as a spreadsheet column to be used for further analysis. Our choice of texture features and program options were the same as Szymanski et al. (2012) and involved calculating a total of 168 texture features spread over the 6 TA methods listed in Table 2. The $[\mu-3\sigma, \mu+3\sigma]$ normalization method was also used, where μ is the mean gray level value and σ the standard deviation. This normalization method has been shown to result in the most consistent output amongst other normalization methods applied prior to TA (Collewet et al., 2004).

Therefore, for each experimental animal, we input four images (masked as described above): left and right CA1 red (HuR) and left and right CA1 green (poly-A), and obtained as the output, 4 columns of 168 rows where each row was a measured texture feature of that respective 8-bit image. The texture features of the left and right CA1 for each poly-A and HuR image were averaged for each experimental animal and each was treated as a single sample for downstream analyses so that each sample gave 2 output TAs: the bilateral average for poly-A and for HuR.

Feature Selection

The next step in TA is feature selection. Because there is redundancy in the 168 measured texture features, and some are not informative for distinguishing the input groups, feature selection is used to find the most informative texture features. This step employs statistical tests to reduce the total number of 168 texture features down to the top 10 optimal set of features that can best distinguish between the experimental groups. The groups being compared are defined beforehand in a "supervised" fashion,

as opposed to an "unsupervised" algorithm which allows the software to automatically divide the samples into groups.

The idea of "supervised" feature selection is very important in the analysis of the present data. The goal is to distinguish the granular staining of reperfused neuronal cytoplasm from the more homogeneous cytoplasmic staining of NICs. Therefore in order to find the texture features that can best make this discrimination, the TA routine is initially run on the two experimental groups that display the extremes of the textures we wish to distinguish. Meaning, we select the sample which contains the most granules in the cytoplasm because it will ultimately provide the greatest difference in appearance from that of a smooth NIC sample which lacks granules. Since the 10I group (as described in Chapter 2) had the greatest mRNA granulation in the poly-A channel (Szymanski et al., 2012), it was run against the NIC for feature selection. The resulting ten features were then subsequently used to test poly-A staining in all experimental groups. Likewise, since the 4I HuR staining showed the most significant granulation, and in fact the only significant granulation for HuR staining in reperfused CA1 neurons, the 4I HuR staining was run against NICs to generate the 10 best texture features for assessing HuR channels in all experimental groups. The experimental groups used for feature selection are summarized in Table 3:

Table 3. Experimental groups used for feature selection by the Fisher test.

	"smooth"	"granular"
poly-A	NIC	10I
HuR	NIC	4I

The top 10 texture features are determined by calculation of the Fisher coefficient (F) for each texture feature in the experimental groups in Table 3. The F coefficient

measures the ratio of between-group variance to within-group variance. The greater the value for the *F* coefficient obtained for a particular texture feature, the better that texture feature is for discriminating between groups. Once determined, the top 10 texture features were isolated for all experimental groups and carried forward for further analysis.

Principle Component Analysis

Once the top 10 features were identified, they were subject to principle component analysis (PCA) as carried out in the MaZda software. PCA is a mathematical technique that allows data contained within a higher dimensional data space (e.g. the 10 dimensional features) to be projected into a lower dimensional space while keeping intact the relative relationship of the higher dimensional data. The resulting lower dimensions are called **principle components**, and in the MaZda software are called "**most expressive features**" (MEF). The principle components are linearly independent variables that are obtained by accounting for the variability that exists among the higher dimensional input variables. The first MEF accounts for the greatest degree of variability among input variables, and any additional MEFs account for any remaining variability until all has been accounted for.

The final step is the conversion of the 10-dimensional feature space into a set of principle components used to describe each image texture. The final data are shown either as plots of individual images on axes of the MEFs, or as averages of the MEFs plotted as bar graphs. MEFs were also analyzed by ANOVA and Tukey post hoc test to detect statistical significance between experimental groups.

Summary of Texture Analysis

The cytoplasmic area of each input image is converted into a set of 168 numbers

that represent the texture of the image. The set of 168 numbers is reduced by the Fisher test to the top 10 numbers that best discriminate the input groups. The set of 10 numbers is further reduced to principle components, or MEFs, which are then interpreted as a numerical representation of the textures contained within the original input images. The MEFs are then analyzed statistically to show differences amongst the experimental groups. Essentially, the entire process of texture analysis is a way to describe the appearance of a microscope image in terms of numerical values. These values can then be compared statistically to reliably quantify differences between microscope images.

3.3.5 Colocalization Analysis

To determine colocalization of poly-A/HuR co-labeling, the optical density method described in Chapter 2 was used. In addition, TA of experimental group yellow channels was also performed, using the methods described above. The input images were the 8-bit gray scale yellow channels calculated in the same manner as described in Chapter 2. For yellow channels, feature selection was based on the three input groups: NIC, 1hR and IPC, and so was on a different basis than the poly-A or HuR TA.

3.4 Results

3.4.1. Qualitative Analysis.

Examples of HuR/poly-A staining of CA1 are shown in Figure 12A. Qualitatively, there were no obvious differences between the 1hR and the IPC groups. Both groups showed mRNA granules in the cytoplasm of the CA1 neurons. Furthermore, both showed a low degree of HuR colocalization with the mRNA granules. But qualitative analysis limited our ability to interpret this data. This motivated us to perform quantitative TA on this dataset.

3.4.2. Quantitative Texture Analysis

The top 10 texture features used to distinguish "granular" from "smooth" staining in the poly-A and HuR channels are shown in Table 4. Again, these features were determined by comparing the experimental groups listed in Table 3. For poly-A, half of the features were from wavelet analysis, two from the autoregressive model, and one each from wavelet analysis, the co-occurrence matrix, and the gradient

Table 4. Top 10 texture features selected by the Fisher Test.

poly-A			HuR		
Texture feature	F	Method	Texture Feature	F	Method
WavEnLH_s-5	14.564	WA	Perc.90%	9.0075	H
GrNonZeros	12.903	GR	Teta2	7.9319	AR
WavEnHL_s-2	12.677	WA	Variance	7.555	H
WavEnHH_s-3	11.675	WA	Teta1	7.3903	AR
Skewness	11.574	H	S(2,2)Entropy	7.0338	CO
WavEnLL_s-1	9.3666	WA	S(2,-2)Entropy	6.5853	CO
Teta1	9.237	AR	S(2,-2)SumEntrp	6.4518	CO
S(2,-2)DifVarnc	8.9064	CO	Vertl_GLevNonU	6.34	CO
Teta2	8.437	AR	45dgr_GLevNonU	6.3265	CO
WavEnLL_s-2	8.3466	WA	Horzl_GLevNonU	6.3183	CO

method. For HuR staining, there were six texture features from the co-occurrence method and two each from the autoregressive and histogram models. Thus, wavelet analysis tended to be the best TA method to distinguish the input groups for poly-A staining, but the co-occurrence matrix method tended to best distinguish HuR granular from non-granular staining.

3.4.3. Texture Analysis of poly-A staining

The main results of TA on poly-A staining are shown in Figure 12B and 12C. PCA reduction of the 10 features in Table 4 resulted in three principle components, MEFs 1, 2 and 3. In Figure 12B, each individual animal is plotted as a point in the 3-dimensional MEF space, and the experimental groups are shown as color-coded clusters (red = NIC; green = 1hR; yellow = IPC). The NIC and 1hR clusters did not overlap, but the IPC cluster overlapped both the NIC and 1hR groups. Figure 12C plots the means ($\pm$ one standard deviation) of each MEF for the experimental groups and

shows the results of ANOVA testing. Only MEF1 cleared statistically at p = 0.0017; post hoc testing showed that the 1hR group was different from NIC and IPC, but the latter two were not statistically different. Thus, while our feature selection was optimized to distinguish the NIC and 1hR groups, the IPC group was intermediate to both in terms of poly-A cytoplasmic texture. The conclusion, based on quantitative TA, that poly-A staining in IPC is intermediate between NIC and 1hR, is not obvious from qualitative inspection of the input images.

3.4.4. Texture Analysis of HuR staining

The analysis of the HuR TA is shown in Figure 12D and 12E. When the 10 best features for distinguishing "granular" from "smooth" HuR staining were applied to the experimental groups, it resulted in a one dimensional MEF space. There was no statistical difference in the HuR texture between the NIC, 1hR and IPC groups. This agrees with the qualitative observation that HuR granules are not apparent in photomicrographs of the 1hR and IPC groups. On this basis, we can conclude that IPC does not enhance HuR colocalization in mRNA granules becase HuR texture after IPC was not different from NICs.

3.4.5. Colocalization Analysis at 1hR with and without IPC

To directly evaluate colocalization of poly-A and HuR in the cytoplasm of the experimental groups, two additonal tests were performed. (1) TA was run on yellow channels and (2) the colocalization method used in Chapter 2 was performed.

Texture analysis of the yellow channels reduced to the one-dimensional MEF1 that statistically separated the NIC from the 1hR group (ANOVA p = 0.02). However, the IPC group overlapped both (Figure 13A), and was not statistically different from either group (Figure 13B). Using the colocalization method described in Chapter 2,

there was no difference in yellow channel OD between any of the experimental groups (Figure 13C; ANOVA p = 0.13).
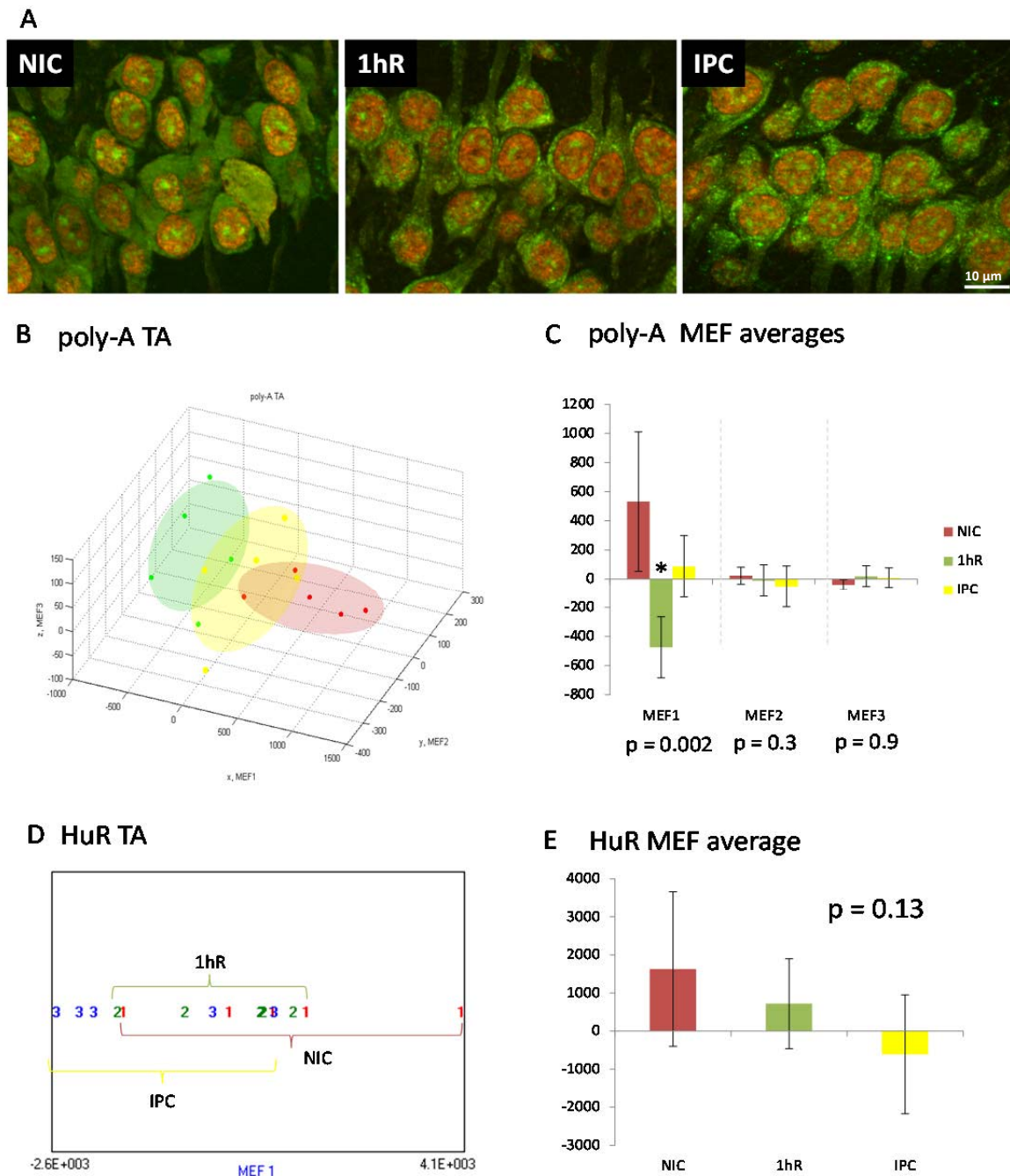
Figure 12. Texture analysis for poly-A and HuR staining. (A) Sample images of NIC, 1hR, and IPC samples from CA1 neurons stained with poly-A (green) and HuR (red). Scale bar in 3rd panel is 10 microns and applies to all three panels. (B) and (D) TA of poly-A and HuR, respectively, where individual samples are plotted in MEF coordinates. "Balloons" in B and brackets in D illustrate how experimental groups cluster. (C) and (E) plot average MEFs (± one standard deviation). ANOVA p values are shown and *

indicates post hoc $p < 0.05$. Red = NIC; green = 1hR; yellow = IPC.
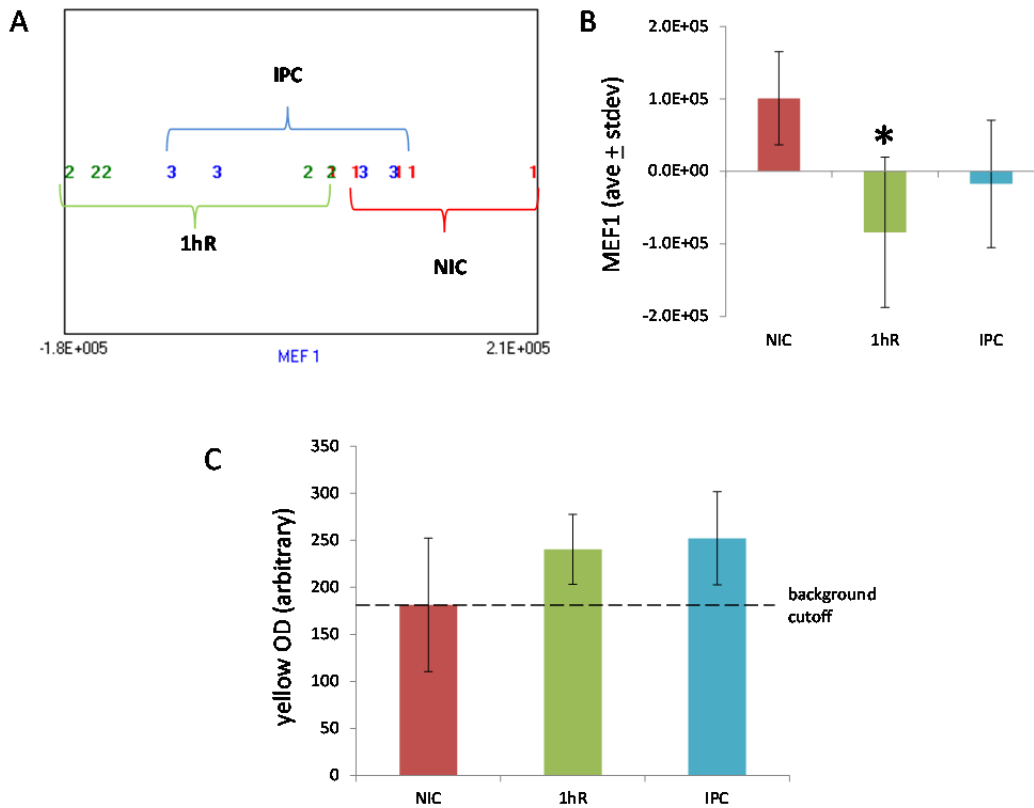
Figure 13. Colocalization Analysis. **(A)** Individual samples were plotted in 1 dimensional MEF1 space. The brackets indicate the clustering of the groups. **(B)** Plots the average MEF values (± one standard deviation). **(C)** The optical density of the yellow channel was measured for each group and those densities are plotted. * ANOVA $p < 0.05$ for NIC vs. 1hR.

3.5 Summary

The studies above were the first to describe the behavior of mRNA granule and HuR staining following IPC. I hypothesized that IPC would enhance the colocalization of mRNA granules with HuR in CA1 neurons following the 2nd ischemic period of 10 min. The data described above do not support this hypothesis, given that (1) HuR granules were not detected after IPC and (2) no increase was observed in colocalization of mRNA granules and HuR in CA1 neurons following IPC, compared to non-IPC 1h reperfused rats. TA of the poly-A, HuR and yellow channels all revealed that a change

does take place in which the IPC samples are quantitatively, with respect to image texture, intermediate to both the NIC and 1hR groups.

CHAPTER 4

Effect of Cycloheximide on mRNA Granules after IPC

4.1 Hypothesis Stated

To date, our knowledge of mRNA granules in post-ischemic neurons is descriptive and correlative. No studies have directly evaluated the functional effect of mRNA granules on post-ischemic outcome. As discussed in Chapter 1, Szymanski et al. (2012) showed that cycloheximide (CHX) pre-treatment attenuated the formation of mRNA granules. Thus, CHX provides a tool to manipulate mRNA granules and study their effect on outcome. In this chapter, studies are described where I gave a single dose of CHX before administration of the 2nd ischemic insult following IPC, and studied: (1) the effect on mRNA granule formation at 1hr reperfusion, and (2) cell survival at 7 days reperfusion after the 2nd ischemic insult. The hypothesis of this final chapter is:

CHX will prevent mRNA granule formation when given after IPC but before the 2nd ischemic insult, and will eliminate the neuroprotective effect of IPC on CA1 neurons.

4.2 Experimental Overview

CHX was administered in a single bolus to two experimental groups: (1) 15 min before a 10 min ischemic insult in previously untreated rats, and (2) 15 min before the 2nd lethal ischemia in rats previously subject to IPC. For each experimental group, half the animals were sacrificed at 1 hr reperfusion and the other half at 7 days reperfusion. The former were stained with poly-A FISH/HuR IF and the latter stained with toluidine blue. TA was performed on the 1 hr reperfused samples, and CA1 was inspected for cell viability in the 7 day group.

4.3 Material and Methods

4.3.1 Materials

CHX was purchased from Sigma Chemical Co. (St. Louis, MO). All other reagents were as described in Chapters 2 and 3.

4.3.2 Animal Model

The non-IPC and IPC surgeries were exactly as described in Chapters 2 and 3, respectively. CHX (1.5 mg/ml) was administered I.P. in 0.25 ml of sterile saline 15 min prior to: (1) the induction of 10 min ischemia in naïve rats (n = 10; 1hR-C), and (2) the induction of 10 min ischemia in rats previously subject to IPC of 2 min ischemia plus 2 days reperfusion (n = 10, IPC-C).

4.3.3 FISH and IF

Half of the 1hR-C and IPC-C rats were sacrificed at 1 hr reperfusion. Perfusion fixation, brain slicing, costaining with poly-A FISH and HuR IF, and microscope imaging were exactly as described in Chapter 2.

4.3.4 Toluidine Blue Staining

The other half of the 1hR-C and IPC-C rats were sacrificed at 7 days reperfusion, perfusion fixed, and brains sectioned in 50 micron slices through the dorsal hippocampus. Toluidine blue staining was performed as described in DeGracia et al. (2007). Brain slices were washed x3 in 0.1 M PBS, mounted onto glass slides with 0.05% gelatin, and air-dried overnight. The following day, the slides were dehydrated using a dilution series of graded ethanol and then incubated in toluidine blue (1:1000) for 20 sec. The excess stain was washed off in a second series of graded ethanol solutions and then washed in 100% xylene. Slides were coverslipped with Permount. Three slides from each animal, at coronal sections of the anterior, middle and posterior

sections of dorsal hippocampus were viewed under a normal bright field microscope under the X20 objective. Each slide was scored in a binary fashion as to whether it did (yes) or did not (no) contain dead CA1 neurons.

4.3.5 Texture Analysis

TA was performed exactly as described in Chapter 3, using the texture features selected by the experimental groups in Table 3, Chapter 3. This allowed determination of the extent to which the CHX-treatment fell on the "smooth" to "granular" spectrum of textures. The TA of CHX-treated groups were compared to the TA of the non-CHX-treated groups described in Chapter 3.

4.4 Results

4.4.1 Qualitative Analysis of Poly-A/HuR Costaining

Similar to the results for CA3 previously reported by the lab (Szymanski et al., 2012), treatment with CHX blunted the formation of mRNA granules in CA1 at 1hr reperfusion in both IPC and non-IPC samples (Figure 14). However, variation amongst animals prevented clear-cut interpretation, so we again applied TA to determine if quantitative differences in cytoplasmic texture could be detected.

4.4.2 TA of CHX-treated samples

Using the texture features in Table 4 to compare the 1hR and 1hR-C groups again led poly-A staining to reduce to a 3D space after PCA. When the individual samples were plotted in the 3D MEF space, the 1hR-C group fell between the NIC and 1hR groups (Figure 15A). When means for MEFs 1-3 were tested against each other by ANOVA, only MEF1 for the NIC and 1hR groups were different. The 1hR-C group was not different from either NIC or 1hR, providing quantitative evidence that the 1hR-C group was intermediate to NICs and 1hR, consistent with an interpretation that CHX

decreased mRNA granule formation at 1 hr reperfusion.

When plotted in the 3D MEF space against the NIC and 1hR groups, the IPC and IPC-C individual samples formed clusters that fell on top of each other, and were also intermediate to the NIC and 1hR groups (Figure 15B). Therefore, by TA quantification, IPC + CHX had no effect on the cytoplasmic texture compared to IPC alone.
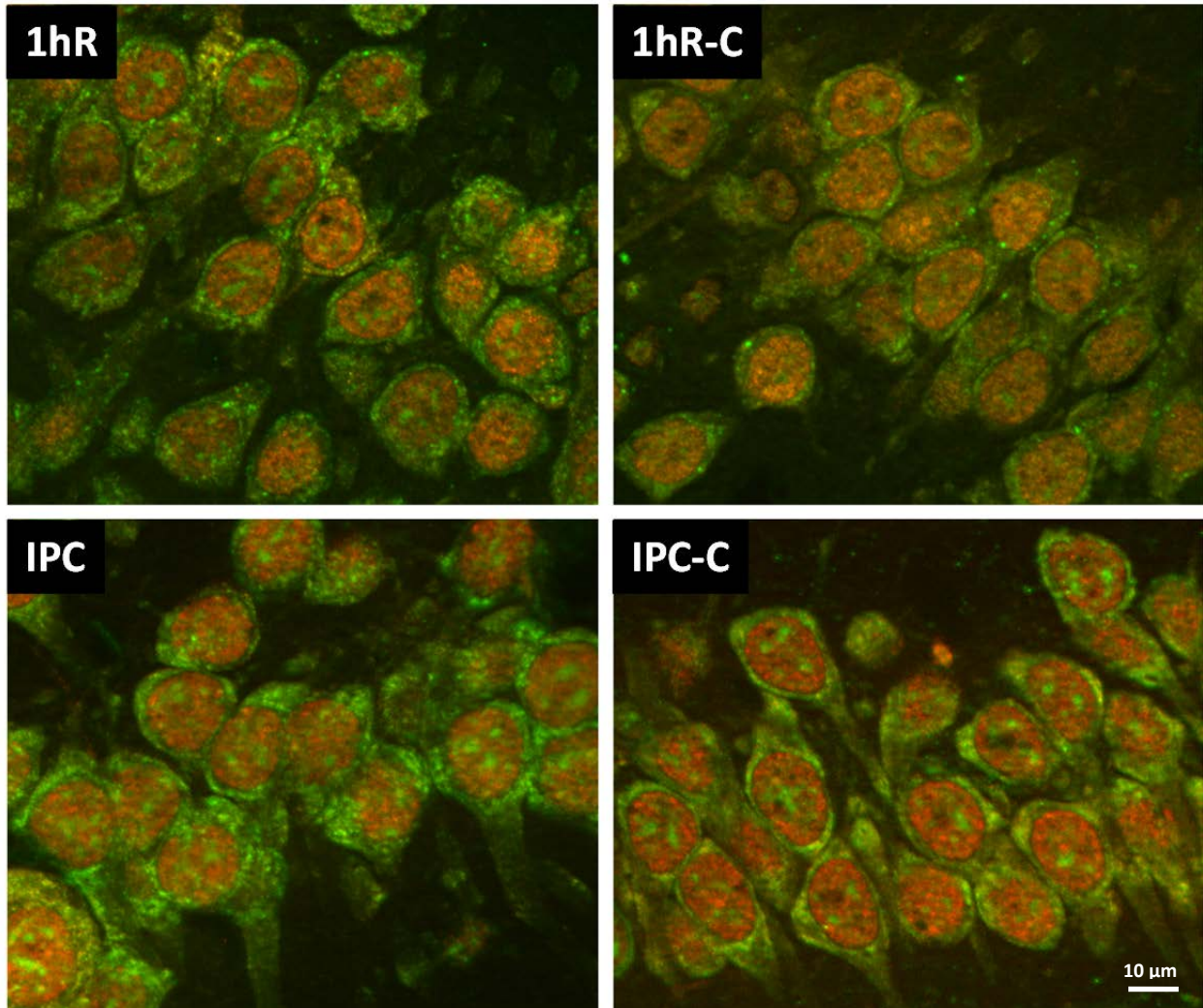
Figure 14. Representative images of samples with and without CHX treatment. The top panels shows the CA1 region following 10 min global ischemia and 1hR without (upper, left) and with (upper, right) CHX. The lower panels show CA1 neurons that underwent IPC without CHX (lower, left) and with CHX (lower, right) 15 min prior to the 2nd ischemic insult.
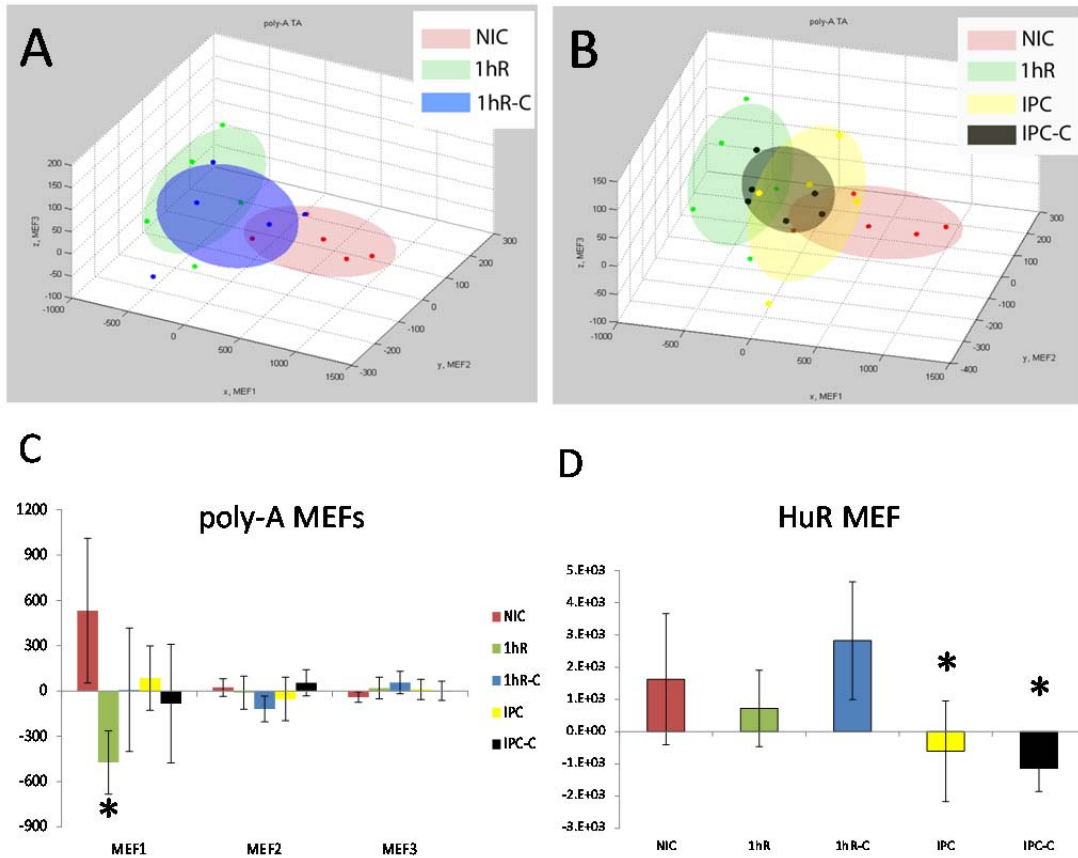
Figure 15. Texture analysis for poly-A and HuR staining. **(A)** and **(B)** TA of poly-A staining where individual samples are plotted in 3D MEF coordinates. Balloons show the clustering of the different experimental groups in relation to one another. **(C)** Plot of the average MEF values for poly-A staining (± one standard deviation). **(D)** Plot of the average MEF values for HuR staining (± one standard deviation) for MEF clusters (not shown). *Tukey post hoc $p < 0.05$ for 1hR vs. NIC in panel C and IPC and IPC-C vs. 1hR-C in panel D.

When performing ANOVA on all five experimental groups for poly-A TA – NIC, 1hR, 1hR-C, IPC and IPC-C, the only statistically significant difference was for MEF1 between the NIC and 1hR group (Figure 15C). Interpreting this in conjunction with qualitative inspection of the microscope images indicates that 1hR-C, IPC and IPC-C all result in cytoplasmic textures intermediate between NIC and 1hR groups. In terms of HuR staining, results from ANOVA on the single MEF1 obtained from PCA, showed that only the 1hR-C group was statistically different from the IPC and IPC-C groups (Figure 15D).

Thus, TA of the microscopic images gives us a quantitative justification to conclude that CHX blunted poly-A mRNA granules in the 1hR group, but had no effect on the IPC group. With respect to the HuR cytoplasmic texture, IPC was not different from the 1hR group, but was different from the 1hR-C group, and there was no texture difference in HuR staining after IPC with or without CHX.

4.4.3 Cell Viability

At 3 days reperfusion after 10 min ischemia, 100% of CA1 neurons die (Figure 16, left). After 7 days reperfusion following IPC plus 10 min ischemia, CA1 completely survives (Figure 16, center). When CHX was administered to the IPC-treated rats, it had no effect on survival and all CA1 neurons survived (Figure 16, right).
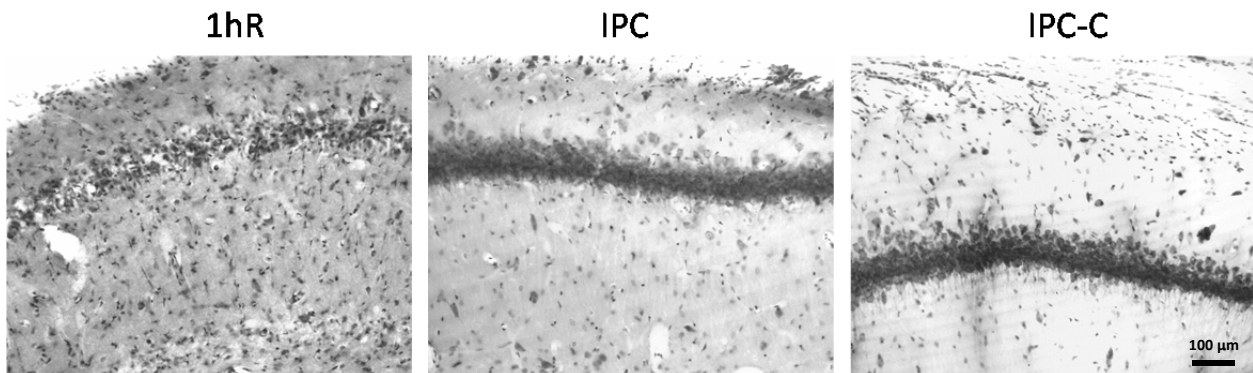
Figure 16. Images showing cell viability with and without IPC. **Left**: Toluidine blue staining demonstrates dying CA1 neurons following 10 min ischemia, 1 hr reperfusion. **Center:** Robust, viable CA1 neurons subject to IPC prior to subsequent 10I, 7DR (7 day reperfusion). **Right:** CA1 neurons following IPC with CHX treatment demonstrate no effect of CHX on cell viability.

4.5 Summary

Administration of CHX 15 min before a lethal 10 min ischemia blunted mRNA granule formation. However, CHX did not alter poly-A or HuR staining when administered 15 min before 10 min ischemia in animals that previously underwent IPC, nor did it have any effect on IPC-induced neuroprotection in CA1 neurons.

CHAPTER 5

Discussion

5.1 Summary of Results

The studies described above were the first ever investigations of mRNA granules following various durations of ischemia and following IPC. A synopsis of the main findings is that, in CA1 neurons:

A. Chapter 2:

    a. mRNA granules formed at 1 hr reperfusion after ischemia durations from 2-10 min.

    b. HuR colocalized with mRNA granules at 1 hr reperfusion following 4 min ischemia, but, as previously shown (Jamison et al., 2008), not after 10 min ischemia.

B. Chapter 3:

    a. By quantitative TA, poly-A mRNA granules at 1 hr reperfusion after IPC were intermediate in texture to the NIC and 1hR groups.

    b. HuR staining did not differ between 1hR and IPC groups.

    c. IPC did not lead to an increase in poly-A mRNA granule colocalization with HuR.

C. Chapter 4:

    a. CHX attenuated mRNA granule formation at 1 hr after 10 min ischemia.

    b. CHX had no effect on mRNA granules formed after IPC.

    c. A single bolus of CHX given 15 min prior to the 2nd 10 min ischemia after IPC did not eliminate the neuroprotective effect of IPC.

These results do not necessarily contradict the main hypothesis of my thesis, that

mRNA granules are a protective response of reperfused neurons. But the results do suggest a more complex picture because some of the specific hypotheses were shown to be wrong. For example, IPC did not enhance HuR colocalization with mRNA granules, and CHX did not decrease the protective effect of IPC. I now discuss how these findings are consistent with the main hypothesis, but at the same time qualify our understanding of the role of mRNA granules in the neuronal response to ischemic injury. In each of the specific discussions, I will also propose future directions relevant to that specific topic.

5.2 Ischemia Duration and mRNA Granules

It is a significant observation that all durations of ischemia from 2-8 min generated mRNA granules in the CA1 and CA3 neurons of individual rats. It is not unreasonable to postulate that the presence of mRNA granules would manifest in a graded response as a function of ischemia duration. However this was not the case, as we did not observe a graded response in the morphology of the mRNA granules. Instead, we observed a binary response where a given experimental animal either did or did not have mRNA granules in their neuronal cytoplasms. However, what did show a graded response was the frequency by which this binary relationship increased as a function of ischemia duration (Figure 8). Meaning, a greater duration of ischemia, would yield a greater number of animals in that particular group with mRNA granules in their cytoplasms.

5.2.1 Curve Fitting

We fit the frequency of mRNA granule formation to both straight lines and the Hill equation, and found the Hill equation to be a better fit (Figure 9). This confirms that mRNA granule formation by itself is not a graded function of ischemic duration and

further justifies interpreting the data in terms of a threshold duration of ischemia at which 50% of mRNA granules form in the experimental animals. By thinking this way, we are comparing to the concept of lethal dose 50% (LD_{50}) used to measure drug responses, where one seeks to find the concentration of a drug that kills 50% of animals exposed to that concentration.

The Hill equation fitting had two free parameters: n, the Hill coefficient, and b, the 50% threshold. When we used the corrected CA3 data, both CA1 and CA3 gave the same value for $b = 1.4$ min of ischemia and the Gaussian curves for b lay directly on top of each other, although CA1 was wider, indicating larger variance among samples. However, the fit gave slightly different values for the Hill coefficient, n: 1.8 for CA1 and 2.1 for CA3. Although, these did not clear statistically, the Gaussian curves were not in perfect alignment, indicating that the difference might indicate something real.

One avenue for future studies would be to measure these curves in a more precise manner and determine if the differences in n are real or just a statistical artifact. This could be accomplished by adding more rats to improve statistical power, and sampling along a tighter time course of ischemia duration, focusing on durations even shorter than 2 min; i.e. 30 sec, 60 sec, 90 sec, and 120 sec. Furthermore, since the current studies were focused solely on the hippocampal CA1 and CA3 neurons, it would be worthwhile to make similar curves for other brain regions and investigate how these neurons respond to varying durations of ischemia. Obtaining values for b and n would provide a more complete picture regarding the threshold of ischemia at which different regions form mRNA granules, if in the same manner at all.

Although the difference in n in the present study was not statistically significant, there is good rationale for investigating it further. The reason why CA1 behaves

differently from CA3 after 10 min ischemia, the former dying and the latter surviving, is currently unknown in spite of years of intense investigation (Lipton, 1999). Dr. DeGracia has recently invented a mathematical model of cell injury (DeGracia et al., 2012) that makes the assumption that the molecular changes inside the injured cells form a **network** of bimolecular interactions. Since the molecules form a network, the interactions connecting the elements hooked together in the network, in principle, can be more or less tightly coupled. We can interpret the value of n in the Hill coefficient to reflect the coupling of the molecules in the network. Given our result that the value for n was less in CA1 compared to CA3, suggests too that the coupling of interactions is less in CA1 than in CA3. This would indicate that CA3 has a more coordinated response to the injury than does CA1. While these ideas are speculative at the moment, they do provide significance to the present result and motivation to follow it through in future studies.

5.2.2 Implications of a "Discreet" Response to mRNA Granule Formation

The observation that mRNA granules formed in a binary fashion, e.g. that an animal either did or did not contain them in its neurons, even in the 2I group, merits further discussion. One implication of this observation is that translation should be almost completely inhibited during the first 1 hr of reperfusion, even after only 2 min ischemia. This suggests a future direction to measure *in vivo* translation at every duration of ischemia and see if there is a graded decrease in translation or not. However, this has already been done: older studies from the 1980s showed that translation is inhibited almost 100% after brief ischemia durations, but that the length of time it took for translation to recover increased with ischemia duration (Dienel et al., 1980). Therefore, it can be seen that our result is consistent with these older studies

and is further supporting evidence that mRNA granules are indicators of TA.

In the present study, we confined the parameters of reperfusion to the 1 hr time point. A possibility for future studies would be to investigate a time course of reperfusion, at each ischemia duration, and evaluate the time it takes for mRNA granules to decay from the cytoplasm. We predict these would parallel protein synthesis rates. The converse would be to look at super-lethal ischemia durations, for example, 20 or 30 min. Such durations of ischemia do not cause DND but cause necrosis. In these cases, we predict no mRNA granules would form because the insult is so great that the resulting damage would overwhelm the neurons to the point they would be incapable of mounting stress responses. Confirmation of these predictions would support the notion that mRNA granules are an intrinsic phase in the neuronal stress response to ischemia.

5.3 HuR/mRNA Granule Colocalization at 4 min Ischemia

Perhaps the most significant finding presented in this thesis is the observation that at low durations of ischemia, HuR colocalized with the poly-A mRNA granules. Although colocalization occurred in the 2I group, we chose to systematically investigate the 4I time point since mRNA granules occurred more frequently in 4I samples than in 2I samples.

Jamison et al. (2008) showed a strict correlation with HuR colocalization to the mRNA granules, and translation of HSP70 protein. It is well-established that CA1 translates HSP70 at sublethal durations of ischemia (Kirino et al., 1991; Sharp et al., 2004; Zhao et al., 2006). Thus, the present findings coupled with those of HSP70 translation reinforce the correlation between HuR colocalization in the mRNA granules and translation of HSP70.

HuR is an mRNA binding protein that binds mRNAs containing an adenine and uridine rich element (ARE) in the 3' untranslated region (Keene, 2007). The *hsp70* mRNA is an ARE-containing mRNA (Gallouzi et al., 2003). Thus, the present data supports the protective role of the mRNA granules, and the idea that they may act as RNA operons to carry out mRNA regulation of stress response programs in the injured neurons.

One important future direction revealed by the present studies is to perform systematic analysis of colocalization at multiple ischemia durations, as opposed to just the 4I and 10I groups studied here. From that point, it would be possible to determine the duration of ischemia at which 50% of animals lack colocalization of HuR in the mRNA granules of CA1 neurons. Given the relationship between colocalization and translation of HSP70, it would follow that at ischemic durations where there is no HuR/mRNA granule colocalization, the neurons would fail to translate heat shock proteins necessary for survival. Thus, it is expected that this information would reveal the threshold duration of ischemia that is lethal to the CA1 neurons, and may ultimately provide an experimental system with which to study the underlying molecular events.

Regarding the questions, "How is the colocalization of HuR and mRNA granules protective?" And "Why is the lack of colocalization associated with a lethal condition?", studies are currently underway in Dr. DeGracia's laboratory by Jeff Szymanski to evaluate patterns of gene expression during reperfusion. He has already shown that there is a predominance of mRNA transcripts that contain AREs upregulated during reperfusion. This suggests regulation of ARE-containing mRNAs is important to post-ischemic outcome. In order to show a causal role of HuR in regulating stress gene transcription, one could do experiments where HuR is knocked out *in vivo* by siRNA,

and then measure cell survival outcome. If the proposed role of HuR in stress gene regulation was in fact valid, it would be expected that knocking out HuR would increase lethality and prevent the translation of intrinsically protective mRNAs after brain I/R.

5.4 Effect of IPC on mRNA Granules

Given that HuR colocalization in mRNA granules is associated with a survival outcome, we were surprised to observe that IPC did not enhance this colocalization. The logic that led us to propose this experimental design was the following. When 10 min ischemia is induced without IPC, HuR and mRNA granules colocalize in CA3 neurons that survive, but do not colocalize in CA1 neurons which inevitably die. Underlying our hypothesis was a model whereby IPC would prevent the intrinsic defect that CA1 suffers from following 10 min ischemia. It is believed that this primary defect prevents the colocalization of HuR in the mRNA granules; a defect which ultimately prevents the translation of HSP70 or other stress proteins. However, our result gives rise to an alternative interpretation. It may be that the IPC stimulus is sufficient to initiate translation of stress genes during the intervening 48 hr period following the initial 2 min ischemia. Effectively, there will be a buildup of stress genes which can then "buffer" the CA1 neurons such that the subsequent 10 min insult no longer delivers the same degree of damage to the CA1 neuron. If the 2nd, 10 min ischemia is less damaging, there is less need for the mRNA granule response, and hence would justify the graded, intermediate response that we observed in the IPC samples, where TA showed them to be intermediate between the NIC and 1hR staining patterns. Taken together, the results suggest that the mRNA granule response in reperfused CA1 neurons may not be such a crucial event following IPC like it is in cells that do not undergo IPC.

It is interesting to note however, based solely on the degree of poly-A granulation as measured by TA, there appears to be more mRNA granulation in the 4I sample, than in the IPC samples, the latter of which had experienced 10 min ischemia. Again, this suggests even the 4 min ischemic insult is experienced as more damaging to the CA1 neurons than a 10 min insult after prior IPC.

A serious limitation that prevents us from over-interpreting this data is the fact that it is based solely upon microscope evidence. Although it is quantified by TA, there is no supporting biochemical data. Thus, to seriously test the ideas entertained here would require biochemical measurements to show: (1) there is less cellular damage in CA1 following IPC plus 10 min ischemia. This could be measured by assaying for lipid peroxidation products or protein aggregates, and (2) upregulation of stress gene proteins already exists at the time the 10 min insult is induced after IPC, which could be measured by Western blot or IH.

Another important future direction to pursue would be to closely investigate the time course of mRNA granule formation during the 48 hr reperfusion period following 2 min ischemia. It is evident that some change is occurring during this critical period, and it ultimately affects how the cell responds to a subsequent 10 min insult. If mRNA granules are shown to form early on within the 48 hr period, it may validate the reason why mRNA granule formation takes on an intermediate profile later when subjected to 10I+1hR following IPC.

The finding that HuR staining was not different between the 1hR and IPC groups, as compared to the NICs, is a significant observation that warrants further discussion. This is a complex issue because, even though the lack of HuR was shown to be constant across these experimental groups, it was not due to the same reasons. In the

case of 1hR samples following a single 10 min ischemic insult, the reason why HuR cannot colocalize with mRNA granules is likely because the cells are so badly damaged, making colocalization impossible. With no colocalization, there can be no translation of HSP70. This is supported by the observation that these neurons invariably die by 72 hrs reperfusion (Jamison et al., 2008).

On the other hand, the CA1 neurons following IPC, may still possess the ability for HuR to colocalize, but perhaps it is simply not necessary because the cells, as discussed earlier, have already been buffered against the damage. Therefore, in this case the HuR colocalization that is necessary to initiate the translation of stress genes is pointless. As such, an essential future direction stemming from this observation would be to systematically investigate the colocalizaton of HuR with mRNA granules during multiple time points within the 48 hr reperfusion period after IPC. Perhaps, if the cell mounts a stress response early on, i.e. following the first 2 min ischemic insult, it would follow that there be colocalization to some extent during this period. As observed in the first experiment, HuR colocalization with mRNA is robust following 4I+1hR. However, extended time points of reperfusion were not tested beyond 1 hr. Following that logic, it is important to look into the entire reperfusion window to get a better sense of exactly when the colocalization occurs and for how long. Moreover, the fact the IPC did not enhance HuR/poly-A colocalization following 10I + 1hR suggests again that the colocalization simply was not needed, or it may have been enhanced at a time point during the 48 hr reperfusion and then dissipated before the subsequent 10I insult.

From my results, it is not accurate to conclude that HuR colocalization behaves the same, meaning it does not occur, following 10I +1hR in animals with and without IPC. In fact if this were the case, the IPC stimulus would not be expected to be

protective. Yet, it is possible that the time point at which HuR colocalizes with mRNA granules is unknown because the reperfusion picture is incomplete. Again, this reinforces the need to further study colocalization during the 48 hr period following the preconditioning stimulus.

5.5 Effect of CHX on mRNA Granules

Based on the TA quantification, CHX blunted mRNA granules in CA1 in the 1hR group, but did not have an effect in the IPC group. Furthermore, the single bolus injection could not block the protective effect of IPC. Similar to the discussion in the previous section, these results suggest that the role of mRNA granules is less important to neuronal outcome following IPC compared to when IPC is absent.

The lab previously showed that CHX attenuated mRNA granules in CA3 following 10 min ischemia and 1 hr reperfusion (Szymanski et al., 2012), and I showed here that the same result held for CA1 neurons after 10 min ischemia without IPC. The response of both CA1 and CA3 to CHX supports the idea that polysome dissociation is upstream from mRNA granule formation since CHX "freezes" polysomes and prevents their dissociation. A confirmatory study would be to measure polysome profiles from CA1 and CA3 in the presence and absence of CHX after 10 min ischemia and 1 hr reperfusion, and show that there are more polysomes in CHX-administered animals.

In contrast to the above results, following exposure to ischemic preconditioning, CHX appeared to have no effect at 1 hr reperfusion after 10 min ischemia. The same logic used in the previous section may also be used to explain this result. If the CA1 neurons are "buffered" as a result of IPC, the subsequent 10 min ischemia should elicit a level of damage that is much less than that of the non-IPC group. Thus, if the insult is less damaging, the formation of protective mRNA granules in neurons will also be less

compared to their counterparts exposed to the full amount of damage. It should follow that in neurons primed with IPC, less mRNA granules would be needed by the cell, and so the effect of CHX at blunting their formation would be less noticeable. Such logic also explains why CHX had no bearing on the protective effect of IPC. If mRNA granules play less of a role in survival outcome after IPC, inhibiting them would not necessarily affect the outcome either. Another interpretation is that the stress responses have already been activated from the preceding 48 hr reperfusion following the initial 2 min insult. If the mRNA granules already formed and set the protective processes in motion, it would make sense that they do not need to form a second time (i.e. following the 2nd ischemic insult). Thus, if they do not form during this period, it is completely irrelevant to administer CHX in the first place because there will be nothing to inhibit.

Thus, in hindsight, which is always 20:20, our results suggest that using IPC with and without CHX turned out not to be an optimal system to study the role of mRNA granules in post-ischemic neuronal outcome. Our results indicate that mRNA granules play a smaller role in determining outcome following the 2nd, usually lethal, ischemic episode after IPC. Or more generally, our results suggest that the 10 min ischemic insult following IPC is experienced and reacted to in a much different fashion by the CA1 neuron, than it is in the absence of prior IPC. However, this insight in itself is relatively novel, for it is commonly thought that the 10 min insult is the same in both instances. The recent demonstration that the patterns of gene expression are different after the 10 min ischemia with and without IPC (Stenzel-Poore et al., 2004; Simon et al., 2007) also points in the same direction of our result. Thus, the work described here deepens the general insight about cell behavior following IPC.

Furthermore, these results are important in that they help widen our perspective

and provide us with future directions to pursue. Biochemical techniques, specifically polysome profiles, will be an important component in moving forward with this work. It was observed that CHX had no effect on the formation of mRNA granules following IPC. This needs to be validated with the use of polysome profiles. Given that the microscope data did not find a quantitative difference in the formation of mRNA granules with and without CHX after IPC, it should follow that, the amount of intact polysomes is also the same between groups with and without CHX in IPC animals.

Finally, another future study following from this experiment would be to repeat the IPC protocol but administer the CHX prior to the 2 min ischemic insult. While this experiment has been done before, and showed that CHX prior to IPC eliminates neuroprotection, the present studies offer a potential explanation for this finding. The current data suggest that translation itself may not be shut off by CHX, because I/R will do that anyway, but instead, the formation of mRNA granules may be prevented. Without the presence of mRNA granules to house the normal mRNA transcripts during stress, the RNA operons will be unable to efficiently carry out their role in expressing the stress responses required for survival. Taken together, it will be essential to further investigate how mRNA granules behave during the 48 hr reperfusion period. Once that role can be established, we will be one step closer to uncovering the mechanism by which ischemic preconditioning confers neuroprotection.

5.6 Summary and Conclusion

Here I described the first studies of mRNA granules following sub-lethal ischemia durations and following IPC. I discovered that mRNA granules behave differently following sub-lethal ischemia than they do following lethal ischemia preceded by IPC. After sublethal ischemia, CA1 behaves much like CA3 does after 10 min ischemia, by

showing colocalization of HuR with the mRNA granules. This is a significant finding since the colocalization correlates to stress gene translation and a survival outcome. The neurons subject to IPC do not show the same behavior as non-IPC neurons, indicating that the prior preconditioning stimulus altered the CA1 neurons so that they do not experience or respond to the 10 min ischemic insult in the same way. The results described here are important for opening up new avenues of investigation on the response of post-ischemic neurons and for deepening our insight about the complexity of this response. Only by a thorough understanding of this complexity will we have a chance to develop clinically effective therapies to halt cardiac arrest and stroke induced brain damage, which to the present, have stubbornly resisted all such efforts.

APPENDIX

WAYNE STATE
UNIVERSITY

ANIMAL WELFARE ASSURANCE # A 3310-01

PROTOCOL # A 01-03-12

Protocol Effective Period: March 8, 2012 – January 31, 2015

TO: Dr. Donald J. DeGracia
Department of Physiology
4116 Scott Hall

FROM: Lisa Anne Polin, Ph.D.
Chairperson
Institutional Animal Care and Use Committee

SUBJECT: Approval of Protocol # A 01-03-12

"Stress Granules Cause Translation Arrest In Ischemic Vulnerable Neurons"

DATE: March 8, 2012

Your animal research protocol has been reviewed by the Wayne State University Institutional Animal Care and Use Committee, and given final approval for the period effective **March 8, 2012** through **January 31, 2015**. The listed source of funding for the protocol is **NIH**. The species and number of animals approved for the duration of this protocol are listed below.

Species	Strain	Qty.	USDA Cat.
RATS	Long Evans, male, 250-300g	126	E
RATS	Long Evans, male, 250-300g	303	D

Be advised that this protocol must be reviewed by the IACUC on an annual basis to remain active. Any change in procedures, change in lab personnel, change in species, or additional numbers of animals requires prior approval by the IACUC. Any animal work on this research protocol beyond the expiration date will require the submission of a new IACUC protocol form and full committee review.

The Guide for the Care and Use of Laboratory Animals is the primary reference used for standards of animal care at Wayne State University. The University has submitted an appropriate assurance statement to the Office for Laboratory Animal Welfare (OLAW) of the National Institutes of Health. The animal care program at Wayne State University is accredited by the Association for Assessment and Accreditation of Laboratory Animal Care International (AAALAC).

REFERENCES

1. Abramoff MD, Magalhães PJ, Ram SJ (2004) Image processing with ImageJ. Biophotonics international 11:36–42.

2. Alparone, L.(1990) Texture-based analysis techniques for the classification of radar images. Radar, Sonar and Navigation, IEE Proceedings. 137(4) 276 - 282.

3. Anderson P, Kedersha N (2006) RNA granules. J Cell Biol 172:803–808.

4. Barone FC, White RF, Spera PA, Ellison J, Currie RW, Wang X, Feuerstein GZ, Rothwell NJ (1998) Ischemic Preconditioning and Brain Tolerance: Temporal Histological and Functional Outcomes, Protein Synthesis Requirement, and Interleukin-1 Receptor Antagonist and Early Gene Expression • Editorial Comment. Stroke 29:1937–1951.

5. Bartus RT, Chen EY, Lynch G, Kordower JH (1999) Cortical ablation induces a spreading calcium-dependent, secondary pathogenesis which can be reduced by inhibiting calpain. Exp Neurol 155:315–326.

6. Bazan NG (1989) Arachidonic acid in the modulation of excitable membrane function and at the onset of brain damage. Ann N Y Acad Sci 559:1–16.

7. Bessert DA, Skoff RP (1999) High-resolution In Situ Hybridization and TUNEL Staining with Free-floating Brain Sections. J Histochem Cytochem 47:693–701.

8. Brengues M, Teixeira D, Parker R (2005) Movement of Eukaryotic mRNAs Between Polysomes and Cytoplasmic Processing Bodies. Science 310:486–489.

9. Burda J, Martín ME, García A, Alcázar A, Fando JL, Salinas M (1994) Phosphorylation of the alpha subunit of initiation factor 2 correlates with the inhibition of translation following transient cerebral ischaemia in the rat. Biochemical Journal 302:335.

10. Collewet G, Strzelecki M, Mariette F (2004) Influence of MRI acquisition protocols and image intensity normalization methods on texture classification. Magn Reson Imaging 22:81–91.

11. Cummings BS, McHowat J, Schnellmann RG (2000) Phospholipase A2s in Cell Injury and Death. J Pharmacol Exp Ther 294:793–799.

12. Danton GH, Dietrich WD (2004) The Search for Neuroprotective Strategies in Stroke. AJNR Am J Neuroradiol 25:181–194.

13. DeGracia DJ (2004) Acute and persistent protein synthesis inhibition following cerebral reperfusion. Journal of Neuroscience Research 77:771–776.

14. DeGracia DJ, Huang Z-F, Huang S (2012) A nonlinear dynamical theory of cell injury. J Cereb Blood Flow Metab 32:1000–1013.

15. DeGracia DJ, Jamison JT, Szymanski JJ, Lewis MK (2008) Translation arrest and ribonomics in post-ischemic brain: layers and layers of players. Journal of Neurochemistry 106:2288–2301.

16. DeGracia DJ, Kumar R, Owen CR, Krause GS, White BC (2002) Molecular Pathways of Protein Synthesis Inhibition During Brain Reperfusion|[colon]| Implications for Neuronal Survival or Death. Journal of Cerebral Blood Flow & Metabolism 22:127–141.

17. DeGracia DJ, Neumar RW, White BC, Krause GS (1996) Global Brain Ischemia and Reperfusion: Modifications in Eukaryotic Initiation Factors Associated with Inhibition of Translation Initiation. Journal of Neurochemistry 67:2005–2012.

18. DeGracia DJ, Rafols JA, Morley SJ, Kayali F (2006) Immunohistochemical mapping of total and phosphorylated eukaryotic initiation factor 4G in rat hippocampus following global brain ischemia and reperfusion. Neuroscience

139:1235–1248.

19. DeGracia DJ, Rudolph J, Roberts GG, Rafols JA, Wang J (2007) Convergence of stress granules and protein aggregates in hippocampal cornu ammonis 1 at later reperfusion following global brain ischemia. Neuroscience 146:562–572.

20. DeGracia DJ, Sullivan JM, Neumar RW, Alousi SS, Hikade KR, Pittman JE, White BC, Rafols JA, Krause GS (1997) Effect of Brain Ischemia and Reperfusion on the Localization of Phosphorylated Eukaryotic Initiation Factor 2α. Journal of Cerebral Blood Flow & Metabolism 17:1291–1302.

21. Dienel G, Pulsinelli W, Duffy T. Regional protein synthesis in rat brain following acute hemispheric ischemia. J Neurochem 1980;35:1216-1226.

22. Demopoulos HB, Flamm ES, Pietronigro DD, Seligman ML (1980) The free radical pathology and the microcirculation in the major central nervous system disorders. Acta Physiol Scand Suppl 492:91–119.

23. Dennis EA (1994) Diversity of Group Types, Regulation, and Function of Phospholipase A2. J Biol Chem 269:13057–13060.

24. Eckstein M, Stratton SJ, Chan LS (2005) Cardiac Arrest Resuscitation Evaluation in Los Angeles: CARE-LA. Ann Emerg Med 45:504–509.

25. Farber JL (1982) Biology of disease: membrane injury and calcium homeostasis in the pathogenesis of coagulative necrosis. Lab Invest 47:114–123.

26. Forcina MS, Farhat AY, O'Neil WW, Haines DE (2009) Cardiac arrest survival after implementation of automated external defibrillator technology in the in-hospital setting. Crit Care Med 37:1229–1236.

27. Freeman BA, Crapo JD (1982) Biology of disease: free radicals and tissue injury. Lab Invest 47:412–426.

28. Gallouzi I, Brennan CM, Steitz JA. Protein ligands mediate the CRM1-dependent export of HuR in response to heat shock. RNA. 2003;9(11):1410.

29. García L, Burda J, Hrehorovská M, Burda R, Martín ME, Salinas M (2004) Ischaemic preconditioning in the rat brain: effect on the activity of several initiation factors, Akt and extracellular signal-regulated protein kinase phosphorylation, and GRP78 and GADD34 expression. Journal of Neurochemistry 88:136–147.

30. Gingras A-C, Raught B, Sonenberg N (1999) eIF4 INITIATION FACTORS: Effectors of mRNA Recruitment to Ribosomes and Regulators of Translation. Annual Review of Biochemistry 68:913–963.

31. Goll DE, Thompson VF, Li H, Wei W, Cong J (2003) The Calpain System. Physiol Rev 83:731–801.

32. Haralick RM, Shanmugam K, Dinstein I (1973) Textural Features for Image Classification. IEEE Transactions on Systems, Man and Cybernetics SMC-3:610 –621.

33. Harrison LCV, Luukkaala T, Pertovaara H, Saarinen TO, Heinonen TT, Järvenpää R, Soimakallio S, Kellokumpu-Lehtinen P-LI, Eskola HJ, Dastidar P (2009) Non-Hodgkin lymphoma response evaluation with MRI texture classification. J Exp Clin Cancer Res 28:87.

34. Hoehner TJ, Garritano AM, Dilorenzo RA, O'Neil BJ, Kumar K, Koehler J, Nayini NR, Huang RR, Krause GS, Aust SD (1987) Brain cortex tissue Ca, Mg, Fe, Na, and K following resuscitation from cardiac arrest in dogs. Am J Emerg Med 5:19– 23.

35. Hossmann KA (1993) Disturbances of cerebral protein synthesis and ischemic

cell death. Prog Brain Res 96:161–177.

36.   Hossmann KA, Kleihues P (1973) Reversibility of ischemic brain damage. Arch Neurol 29:375–384.

37.   Hu BR, Wieloch T (1993) Stress-induced inhibition of protein synthesis initiation: modulation of initiation factor 2 and guanine nucleotide exchange factor activities following transient cerebral ischemia in the rat. J Neurosci 13:1830–1838.

38.   Jamison JT, Kayali F, Rudolph J, Marshall M, Kimball SR, DeGracia DJ (2008) Persistent redistribution of poly-adenylated mRNAs correlates with translation arrest and cell death following global brain ischemia and reperfusion. Neuroscience 154:504–520.

39.   Jamison JT, Lewis MK, Kreipke CW, Rafols JA, DeGracia DJ (2011) Polyadenylated mRNA staining reveals distinct neuronal phenotypes following endothelin 1, focal brain ischemia, and global brain ischemia/ reperfusion. Neurol Res 33:145–161.

40.   Kato H, Liu Y, Araki T, Kogure K (1991) Temporal profile of the effects of pretreatment with brief cerebral ischemia on the neuronal damage following secondary ischemic insult in the gerbil: cumulative damage and protective effects. Brain Res 553:238–242.

41.   Kayali F, Montie HL, Rafols JA, DeGracia DJ (2005) Prolonged translation arrest in reperfused hippocampal cornu Ammonis 1 is mediated by stress granules. Neuroscience 134:1223–1245.

42.   Kedersha N, Stoecklin G, Ayodele M, Yacono P, Lykke-Andersen J, Fritzler MJ, Scheuner D, Kaufman RJ, Golan DE, Anderson P (2005) Stress granules and processing bodies are dynamically linked sites of mRNP remodeling. J Cell Biol

169:871–884.

43. Keene JD (2007) RNA regulons: coordination of post-transcriptional events. Nature Reviews Genetics 8:533–543.

44. Kirino T (1982) Delayed neuronal death in the gerbil hippocampus following ischemia. Brain Res 239:57–69.

45. Kirino T, Tsujita Y, Tamura A (1991) Induced tolerance to ischemia in gerbil hippocampal neurons. J Cereb Blood Flow Metab 11:299–307.

46. Kitagawa K, Matsumoto M, Kuwabara K, Tagaya M, Ohtsuki T, Hata R, Ueda H, Handa N, Kimura K, Kamada T (1991) "Ischemic tolerance" phenomenon detected in various brain regions. Brain Res 561:203–211.

47. Kleihues P, Hossmann KA (1971) Protein synthesis in the cat brain after prolonged cerebral ischemia. Brain Res 35:409–418.

48. Krause GS, White BC, Aust SD, Nayini NR, Kumar K (1988) Brain cell death following ischemia and reperfusion: a proposed biochemical sequence. Crit Care Med 16:714–726.

49. Kumar R, Krause GS, Yoshida H, Mori K, DeGracia DJ (2003) Dysfunction of the unfolded protein response during global brain ischemia and reperfusion. J Cereb Blood Flow Metab 23:462–471.

50. Lipton P (1999) Ischemic Cell Death in Brain Neurons. Physiol Rev 79:1431–1568.

51. Lloyd-Jones D et al. (2009) Heart disease and stroke statistics--2009 update: a report from the American Heart Association Statistics Committee and Stroke Statistics Subcommittee. Circulation 119:e21–181.

52. Losa GA, Castelli C (2005) Nuclear patterns of human breast cancer cells during

apoptosis: characterisation by fractal dimension and co-occurrence matrix statistics. Cell Tissue Res 322:257–267.

53.   Lyden P, Wahlgren NG (2000) Mechanisms of action of neuroprotectants in stroke. Journal of Stroke and Cerebrovascular Diseases 9:9–14.

54.   Martín de la Vega C, Burda J, Nemethova M, Quevedo C, Alcázar A, Martín ME, Danielisova V, Fando JL, Salinas M (2001) Possible mechanisms involved in the down-regulation of translation during transient global ischaemia in the rat brain. Biochem J 357:819–826.

55.   Martínez-Sánchez M, Striggow F, Schröder UH, Kahlert S, Reymann KG, Reiser G (2004) Na+ and Ca2+ homeostasis pathways, cell death and protection after oxygen–glucose-deprivation in organotypic hippocampal slice cultures. Neuroscience 128:729–740.

56.   McCord JM (1993) Oxygen-derived free radicals. New Horiz 1:70–76.

57.   Merrick WC (1990) Overview: mechanism of translation initiation in eukaryotes. Enzyme 44:7–16.

58.   Mies G, Paschen W, Hossmann K-A (1990) Cerebral Blood Flow, Glucose Utilization, Regional Glucose, and ATP Content During the Maturation Period of Delayed Ischemic Injury in Gerbil Brain. Journal of Cerebral Blood Flow & Metabolism 10:638–645.

59.   Montie HL, Haezebrouck AJ, Gutwald JC, DeGracia DJ (2005) PERK is activated differentially in peripheral organs following cardiac arrest and resuscitation. Resuscitation 66:379–389.

60.   Muir KW, Buchan A, von Kummer R, Rother J, Baron J-C (2006) Imaging of acute stroke. Lancet Neurol 5:755–768.

61. Murakami M, Nakatani Y, Atsumi G, Inoue K, Kudo I (1997) Regulatory functions of phospholipase A2. Crit Rev Immunol 17:225–283.

62. Nakamura T, Minamisawa H, Katayama Y, Ueda M, Terashi A, Nakamura K, Kudo Y (1999) Increased intracellular Ca2+ concentration in the hippocampal CA1 area during global ischemia and reperfusion in the rat: a possible cause of delayed neuronal death. Neuroscience 88:57–67.

63. Neumar RW, DeGracia DJ, Konkoly LL, Khoury JI, White BC, Krause GS (1998) Calpain mediates eukaryotic initiation factor 4G degradation during global brain ischemia. J Cereb Blood Flow Metab 18:876–881.

64. Neumar RW, Meng FH, Mills AM, Xu YA, Zhang C, Welsh FA, Siman R (2001) Calpain Activity in the Rat Brain after Transient Forebrain Ischemia. Experimental Neurology 170:27–35.

65. O'Collins VE, Macleod MR, Donnan GA, Horky LL, van der Worp BH, Howells DW (2006) 1,026 experimental treatments in acute stroke. Ann Neurol 59:467–477.

66. Oldfield S, Jones BL, Tanton D, Proud CG (1994) Use of monoclonal antibodies to study the structure and function of eukaryotic protein synthesis initiation factor eIF-2B. European Journal of Biochemistry 221:399–410.

67. Olney JW (1990) Excitotoxic Amino Acids and Neuropsychiatric Disorders. Annual Review of Pharmacology and Toxicology 30:47–71.

68. Paschen W (1996) Disturbances of calcium homeostasis within the endoplasmic reticulum may contribute to the development of ischemic-cell damage. Medical Hypotheses 47:283–288.

69. Pérez-Pinzón MA (2004) Neuroprotective Effects of Ischemic Preconditioning in

Brain Mitochondria Following Cerebral Ischemia. Journal of Bioenergetics and Biomembranes 36:323–327.

70. Pérez-Pinzón MA, Xu GP, Dietrich WD, Rosenthal M, Sick TJ (1997) Rapid preconditioning protects rats against ischemic neuronal damage after 3 but not 7 days of reperfusion following global cerebral ischemia. J Cereb Blood Flow Metab 17:175–182.

71. Pestka S (1971) Inhibitors of Ribosome Functions. Annual Review of Microbiology 25:487–562.

72. Pietikäinen (editor) (2000) Texture Analysis In Machine Vision. Series in Machine Perception and artificial Intelligence: Volume 40. ISBN: 978-981-02-4373-9 World Scientific Publishing Co., Inc.Hackensack, NJ.

73. Puisieux F, Deplanque D, Bulckaen H, Maboudou P, Gelé P, Lhermitte M, Lebuffe G, Bordet R (2004) Brain ischemic preconditioning is abolished by antioxidant drugs but does not up-regulate superoxide dismutase and glutathion peroxidase. Brain Research 1027:30–37.

74. Roger VL et al. (2011) Heart disease and stroke statistics--2011 update: a report from the American Heart Association. Circulation 123:e18–e209.

75. Rowlands AG, Panniers R, Henshaw EC (1988) The catalytic mechanism of guanine nucleotide exchange factor action and competitive inhibition by phosphorylated eukaryotic initiation factor 2. J Biol Chem 263:5526–5533.

76. Sairanen T, Ristimäki A, Karjalainen-Lindsberg ML, Paetau A, Kaste M, Lindsberg PJ (1998) Cyclooxygenase-2 is induced globally in infarcted human brain. Ann Neurol 43:738–747.

77. Sattler R, Tymianski M (2001) Molecular mechanisms of glutamate receptor-

mediated excitotoxic neuronal cell death. Mol Neurobiol 24:107–129.

78. Schwartz DC, Parker R (2000) mRNA Decapping in Yeast Requires Dissociation of the Cap Binding Protein, Eukaryotic Translation Initiation Factor 4E. Mol Cell Biol 20:7933–7942.

79. Sengottuvelan, P. (2008) Performance of Decamouflaging Through Exploratory Image Analysis. In PR Bajaj (editor) Emerging Trends in Engineering and Technology, 2008. ICETET '08. pg 6-10.

80. Sharp F, Ran R, Lu A, Tang Y, Strauss K, Glass T, Ardizzone T, Bernaudin M (2004) Hypoxic preconditioning protects against ischemic brain injury. Neurotherapeutics 1:26–35.

81. Siemkowicz E, Hansen AJ (1981) Brain Extracellular Ion Composition and EEG Activity Following 10 Minutes Ischemia in Normo- and Hyperglycemic Rats. Stroke 12:236–240.

82. Silver IA, Erecińska M (1990) Intracellular and extracellular changes of [Ca2+] in hypoxia and ischemia in rat brain in vivo. J Gen Physiol 95:837–866.

83. Simon R, Henshall D, Stoehr S, Meller R (2007) Endogenous mechanisms of neuroprotection. Epilepsia 48 Suppl 8:72–73.

84. Smith ML, Auer RN, Siesjö BK (1984) The density and distribution of ischemic brain injury in the rat following 2-10 min of forebrain ischemia. Acta Neuropathol 64:319–332.

85. Sonenberg N, Dever TE (2003) Eukaryotic translation initiation factors and regulators. Curr Opin Struct Biol 13:56–63.

86. Stenzel-Poore MP, Stevens SL, Simon RP (2004) Genomics of Preconditioning. Stroke 35:2683–2686.

87.   Stetler RA, Zhang F, Liu C, Chen J (2009) Ischemic tolerance as an active and intrinsic neuroprotective mechanism. Handb Clin Neurol 92:171–195.

88.   Sun GY, Xu J, Jensen MD, Simonyi A (2004) Phospholipase A2 in the Central Nervous System Implications for Neurodegenerative Diseases. J Lipid Res 45:205–213.

89.   Szczypiński PM, Strzelecki M, Materka A, Klepaczko A (2009) MaZda--a software package for image texture analysis. Comput Methods Programs Biomed 94:66–76.

90.   Szymanski JJ, Jamison JT, DeGracia DJ (2012) Texture analysis of poly-adenylated mRNA staining following global brain ischemia and reperfusion. Computer Methods and Programs in Biomedicine 105:81–94.

91.   Tenenbaum SA, Lager PJ, Carson CC, Keene JD (2002) Ribonomics: identifying mRNA subsets in mRNP complexes using antibodies to RNA-binding proteins and genomic arrays. Methods 26:191–198.

92.   Uppal SO, Voronine DV, Wendt E, Heckman CA (2010) Morphological fractal analysis of shape in cancer cells treated with combinations of microtubule-polymerizing and -depolymerizing agents. Microsc Microanal 16:472–477.

93.   White BC, Grossman LI, Krause GS (1993) Brain injury by global ischemia and reperfusion: a theoretical perspective on membrane damage and repair. Neurology 43:1656–1665.

94.   White BC, Sullivan JM, DeGracia DJ, O'Neil BJ, Neumar RW, Grossman LI, Rafols JA, Krause GS (2000) Brain ischemia and reperfusion: molecular mechanisms of neuronal injury. Journal of the Neurological Sciences 179:1–33.

95.   Wiegand F, Liao W, Busch C, Castell S, Knapp F, Lindauer U, Megow D, Meisel

A, Redetzky A, Ruscher K, Trendelenburg G, Victorov I, Riepe M, Diener HC, Dirnagl U (1999) Respiratory Chain Inhibition Induces Tolerance to Focal Cerebral Ischemia. Journal of Cerebral Blood Flow & Metabolism 19:1229–1237.

96. Zhao J, Sun S, Chen X (2006) Protective effects of focal ischemic preconditioning and HSP70 expression on middle cerebral artery occlusion in rats. J Huazhong Univ Sci Technol Med Sci 26:436–439.

97. Zook JM, Iftekharuddin KM (2005) Statistical analysis of fractal-based brain tumor detection algorithms. Magnetic Resonance Imaging 23:671–678.

ABSTRACT

mRNA GRANULES AND ISCHEMIC PRECONDITIONING

by

MICHELLE R. SMITH

December 2012

Advisor: Donald J. DeGracia, Ph.D.

Major: Physiology

Degree: Master of Science

Brain ischemia and reperfusion that occurs after stroke and cardiac arrest, causes translation arrest (TA) in neurons which is irreversible in neurons that will undergo delayed neuronal death. TA is linked to mRNA granules, which are involved in ischemia-induced stress genes translation. Ischemic preconditioning (IPC) is the most protective response known that protects neurons from a lethal ischemic insult. In this thesis I studied the effects of (1) sublethal durations of ischemia, (2) IPC and (3) cycloheximide (CHX) on the formation of mRNA granules at 1 hour of reperfusion and the colocalization of HuR in the mRNA granules. All durations tested, from 2 to 8 min ischemia caused formation of mRNA granules, and HuR colocalized in the mRNA granules at lower ischemia durations in CA1 neurons. However, IPC appeared to attenuate the formation of mRNA granules at 1 hour reperfusion and did not enhance HuR colocalization. CHX inhibited mRNA granules at 1 hour reperfusion, but had no effect in animals subjected to prior IPC. These results show that sublethal durations of ischemia cause CA1 neurons to behave similarly to CA3 neurons. However, the mRNA granule response appears to be less important after a 10 min ischemia in preconditioned animals. These results show that the 10 min ischemia period is

perceived differently by the preconditioned CA1 neuron compared to a non-preconditioned neuron. Moreover, these results shed important light on the post-ischemic neuronal response, and will help in the effort to develop effective therapies to protect against stroke and cardiac arrest brain damage.

AUTOBIOGRAPHICAL STATEMENT

MICHELLE R. SMITH

Education
- Wayne State University, Detroit, MI
  - Master of Science in Physiology. Expected graduation: August 2012
- University of Michigan, Ann Arbor, MI
  - Bachelor of Science in Brain, Behavior, & Cognitive Science, April 2008

Research Experience:

11/2010-8/2012   Wayne State University School of Medicine, Detroit, MI
Dept. of Physiology, DeGracia Laboratory – PI: Dr. Donald DeGracia
Investigated the stress response and damage mechanisms in the cortex and hippocampus following global ischemia. Performed perfusion fixation, vibratome sectioning, and Immunofluorescence-FISH techniques to visualize these specific brain regions of interest following 10 minute ischemia and 1-72 hour reperfusion.

9/2009-7/2010   University of Michigan Medical School, Ann Arbor, MI
Department of Physiology, Borjigin Laboratory – PI: Dr. Jimo Borjigin
Isolated mutations in the ATP7B gene in rat models to understand circadian disturbances in Wilson's disease. Used implantable telemetry to follow physiological parameters during light-dark cycles to uncover additional control mechanisms of circadian rhythms. Maintained care of large rat colony for use in various studies, and maintained overall organization of lab space.

5/2006-1/2009   University of Michigan, Ann Arbor, MI
Molecular and Behavioral Neuroscience Institute – PI: Dr. Juan Lopez
Performed DNA isolation and PCR to explore the expression of serotonin receptors in transgenic mouse models. Investigated neuroanatomical structures through sectioning and mRNA expression involved in depressive disorders using In Situ Hybridization

10/2005-4/2006   University of Michigan, Ann Arbor, MI
Department of Psychology, Faculty Laboratory – PI: Dr. Theresa Lee
Performed capsule implant surgeries and gonadectomies on degus to study hormonal regulation of circadian rhythms. Collected data using Vital View Software and quantified results using Actiview Biological Rhythms Software. Scored and tabulated circadian rhythm data into database for 30-40 degus during three developmental stages and two different light cycles.

Honors and Awards:
- Golden Key International Honour Society (2011)
- Donald R. Shepherd Scholarship, University of Michigan Marching Band (2006)
- Taubman Endowment Scholarship, University of Michigan Marching Band (2005)

Presentations:
1. Zhang LS**, Smith MR**, Liu T, Borjigin J.Photoperiod and Jet Lag: Influence of Pineal Melatonin Onset Timing on Reentrainment Rate of Rats. Poster session. *Wayne State University & University of Michigan 1st Annual Joint Physiology Symposium.* Detroit, Michigan. August 20, 2010.